

University of Windsor

## Scholarship at UWindor

---

Electronic Theses and Dissertations

Theses, Dissertations, and Major Papers

---

1-1-1963

### Paramagnetic resonance in solids.

John W. Carswell  
*University of Windsor*

Follow this and additional works at: <https://scholar.uwindsor.ca/etd>

---

#### Recommended Citation

Carswell, John W., "Paramagnetic resonance in solids." (1963). *Electronic Theses and Dissertations*. 6324.  
<https://scholar.uwindsor.ca/etd/6324>

This online database contains the full-text of PhD dissertations and Masters' theses of University of Windsor students from 1954 forward. These documents are made available for personal study and research purposes only, in accordance with the Canadian Copyright Act and the Creative Commons license—CC BY-NC-ND (Attribution, Non-Commercial, No Derivative Works). Under this license, works must always be attributed to the copyright holder (original author), cannot be used for any commercial purposes, and may not be altered. Any other use would require the permission of the copyright holder. Students may inquire about withdrawing their dissertation and/or thesis from this database. For additional inquiries, please contact the repository administrator via email ([scholarship@uwindsor.ca](mailto:scholarship@uwindsor.ca)) or by telephone at 519-253-3000ext. 3208.

PARAMAGNETIC RESONANCE IN SOLIDS

BY

JOHN W. CARSWELL

A Thesis

Submitted to the Faculty of Graduate Studies through the  
Department of Physics in Partial Fulfillment  
of the Requirements for the Degree of  
Master of Science at Assumption  
University of Windsor

Windsor, Ontario

1963

UMI Number: EC52503

### INFORMATION TO USERS

The quality of this reproduction is dependent upon the quality of the copy submitted. Broken or indistinct print, colored or poor quality illustrations and photographs, print bleed-through, substandard margins, and improper alignment can adversely affect reproduction.

In the unlikely event that the author did not send a complete manuscript and there are missing pages, these will be noted. Also, if unauthorized copyright material had to be removed, a note will indicate the deletion.

**UMI**<sup>®</sup>

---

UMI Microform EC52503

Copyright 2008 by ProQuest LLC.

All rights reserved. This microform edition is protected against unauthorized copying under Title 17, United States Code.

ProQuest LLC  
789 E. Eisenhower Parkway  
PO Box 1346  
Ann Arbor, MI 48106-1346

AA 46871

Approved

N. E. Hedgecock  
Dr. N. E. Hedgecock

S. N. Kalra  
Dr. S. N. Kalra

F. Holuj  
Dr. F. Holuj  
(Supervisor)

73718

## ABSTRACT

In this paper our study was twofold. One, we investigated the effect of x-rays on a single crystal of calcite ( $\text{CaCO}_3$ ) by means of paramagnetic resonance techniques at liquid air temperatures. Two, we investigated the paramagnetic impurities in a single crystal of spodumene ( $\text{LiAl}(\text{SiO}_3)_2$ ).

In the investigation of calcite we irradiated the calcite with the most intense and the strongest x-rays available for periods of at least 10 hours at room temperatures. We were looking for the creation of paramagnetic centers in the single crystals of calcite. Our results for calcite were negative; there was no observed spectrum produced by x-ray irradiation. We have been able to state a number of reasons for this negative result. First, there were no paramagnetic centers produced; hence there would not be any spectra observed. Second, if there were paramagnetic centers produced it was possible that the relaxation time for the spin system was not sufficiently long, consequently the resonance line would be very broad and thus it would be obscured. Third, it was possible that the Zeeman sublevels were not adequately populated to give an observable effect.

The work done on spodumene has produced a number of results. First, there was observed a spectrum and it was attributed to the  $\text{Fe}^{+3}$  ion. Second, one line of the spectrum

has been analyzed and it was thought to be due to the  $-1/2$  to  $1/2$  transition. Third, the principal values of the g-factor for axial symmetry were found to be

$$g_{\perp} = 3.619 \quad \text{and} \quad g_{\parallel} = 1.960$$

Fourth, there was also observed in the iron paramagnetic spectrum a hyperfine structure produced by the interaction of the nuclear magnetic moments of aluminium and lithium with the spin magnetic moment of the iron ion.

## ACKNOWLEDGEMENTS

I would like to express my appreciation to Dr. F. Holuj for the suggestion of the problem, for the helpful supervision of my work and the aid offered me in the preparation of the thesis. Also I am grateful to Mr. W. Grewe for the construction of the precision goniometer and the liquid air cryostat.

## TABLE OF CONTENTS

	Page
ABSTRACT	ii
ACKNOWLEDGEMENTS	iv
Chapter	
I. INTRODUCTION	1
II. THEORY	6
III. APPARATUS	17
IV. EXPERIMENTAL PROCEDURE AND RESULTS	43
V. CONCLUSIONS	56
BIBLIOGRAPHY	58
VITA AUCTORIS	59



## LIST OF TABLES

	Page
Table	
1. DATA OF THE RESONANCE LINE FOR THE X, Y, AND Z ORIENTATIONS	52
2. DATA FOR CALCULATION OF $g_{\perp}$ AND $g_{\parallel}$	54

## LIST OF ILLUSTRATIONS

Figure	Page
1. SIXFOLD TETRAGONAL SYMMETRY (Chap. II)	11
2. THE SPLITTING OF THE GROUND STATE IN A CUBIC FIELD	13
3. SPLITTING IN A TETRAGONAL FIELD	13
1. ELECTRON SPIN SPECTROMETER (Chap. III)	18
2. 30 Mc/s AMPLIFIER AND DETECTOR	20
3. 200 c/s AMPLIFIER	22
4. LOCK-IN DETECTOR	23
5. 30 Mc/s AMPLIFIER	25
6. PHASE DETECTOR	25
7. 10k c/s AMPLIFIER	26
8. PHASE DETECTOR	28
9. 10k c/s OSCILLATOR	29
10. KLYSTRON POWER SUPPLY	31
11. 200 c/s OSCILLATOR	33
12. POWER AMPLIFIER	34
13. ENVELOPE OF CRYOSTAT	36
14. CRYOSTAT	37
15. CAVITIES	39
16. PROJECTION OF UNIT CELL OF SPODUMENE	48
17. ANGULAR VARIATION OF A SINGLE RESONANCE LINE	51
18. THE RESONANCE SPECTRUM OF $\text{Fe}^3$	55

# I

## INTRODUCTION

Paramagnetic resonance, also known as electron-spin resonance, was first observed by Zavoisky in 1945. Using a radio-frequency field at 25 meters, he induced magnetic dipole transitions among electronic Zeeman levels in a paramagnetic center. The line widths were 50 gauss or larger, and consequently a resonance line was scarcely discernible at such a low frequency. This corresponded to a resonance peak at 4 gauss. In Zavoisky's second series of experiments he found a resonance line for the paramagnetic copper ion,  $\text{Cu}^{+2}$ , at 47.7 gauss by using a frequency of 133 Mc/s. The paramagnetic copper ion in  $\text{CuCl}_2 \cdot 2\text{H}_2\text{O}$  gave a g-factor of two. Finally Zavoisky conducted experiments in the microwave region and observed clearly resolved resonance lines of 200 to 300 gauss in width, while using a steady magnetic field of one kilogauss. In the U.S.A., R. L. Cummmerow and D. Halliday observed well resolved resonance lines of the paramagnetic ion manganese in 173 grams of  $\text{MnSO}_4 \cdot 4\text{H}_2\text{O}$ . They used a microwave resonance cavity excited at 2,930 Mc/s. In 1947 at the Claredon Laboratory, Bagguley and Griffiths observed the resonances of the paramagnetic ion of chromium in a chrome alum crystal,  $\text{KCr}(\text{SO}_4)_2 \cdot 12\text{H}_2\text{O}$ , at 3.18 cm. Sub-

sequently, much work was done in the field of paramagnetic resonance. The experimental techniques and apparatus were perfected by the Oxford group, headed by Bleaney and Griffiths, while the work of Pryce and his co-workers advanced the theoretical understanding of the subject.

There are a number of different instances wherein electronic paramagnetism occurs. They are as follows: (1) in all atoms having an odd number of electrons, such as in atomic hydrogen; (2) in ions having partly filled inner electronic shells as in the transition groups; (3) in molecules having an odd number of electrons, such as in NO; (4) in a small number of molecules with an even number of electrons but having a resultant orbital angular momentum, as in  $O_2$ ; (5) in free radicals, possessing an unpaired electron, as in  $CH_3$ . (6) Also unpaired electrons can be produced in solutions or solids by irradiation with light, x-rays,  $\gamma$ -rays or with energetic particles.

The energy of a free paramagnetic ion placed in an external magnetic field  $\vec{H}$  and possessing a magnetic moment  $\vec{\mu}$  and a resultant angular momentum  $\vec{J}$  is:  $E = -\vec{\mu} \cdot \vec{H}$  (1)

This formula expresses the energy due to the action of a torque caused by  $\vec{H}$  on the magnetic momentum vector. According to quantum mechanics, the vector  $\vec{J}$  acted on by a strong magnetic field is quantized along the magnetic field direction. The components of  $\vec{J}$  along the magnetic field direction take on the values:  $-J, -J+1, \dots, J-1, J$ .

We can also write down the magnetic moment:

$$\vec{\mu} = -g \frac{e}{2mc} \vec{J} \hbar = -g \frac{e \hbar}{4\pi mc} \vec{J} = -g \beta \vec{J} \quad (2)$$

Here  $g$  is called the  $g$ -factor and  $\beta$  is the Bohr magneton.

Substituting eqn. (2) into eqn. (1), we get

$$E = g \beta \vec{J} \cdot \vec{H} = g \beta J H \cos(J, H) \quad (3)$$

Since  $J \cos(J, H)$  is the projection of  $\vec{J}$  on  $\vec{H}$  and since  $\vec{J}$  has  $(2J+1)$  projections, we shall write  $J \cos(J, H)$  as  $M_J$ .

$$E = g \beta H M_J \quad \text{where } M_J : -J, -J+1, \dots, J-1, J \quad (4)$$

The energy difference between adjacent  $M_J$  states is

$$\Delta E = g \beta H (M_{J_2} - M_{J_1}) = g \beta H \text{ for } \Delta M_J = \pm 1 \quad (5)$$

If we place an oscillating magnetic field of frequency  $\nu$ , such that  $h\nu$  is equal to the energy difference  $\Delta E$ , then there occurs a magnetic dipole transition between two adjacent  $M_J$  states. Those transitions that reach the higher energy states absorb energy from the oscillating electromagnetic field and those that reach the lower energy state emit energy to the oscillating field. Relation (5) becomes for paramagnetic resonance

$$h\nu = g \beta H \quad (6)$$

Formula (6) expresses the resonance conditions.

The probabilities, for emission and absorption, in the presence of an intense alternating electromagnetic field are equal. But by Boltzmann's statistics, there are more electrons in the lower energy state than there are in the higher energy state. Consequently, there is observed a net absorption of microwave energy.

The literature on paramagnetic resonance is very extensive. Low's book (1960) on paramagnetic resonance in solids gives the present state of the work being done in this field. Most of the work has been done in a class of substances which belong to the cubic symmetry group and in these cases, all of the features of paramagnetic resonance can be explained theoretically. It is when the symmetry of the site of the paramagnetic ion in question is not cubic that many of the unexplained features appear. This is the result of the admixture of the excited states with the ground state. Before these unexplained aspects are clarified much experimental work must be done.

At the outset of the present work, the task was to detect and study the excitation centers of x-ray irradiated crystals by paramagnetic resonance techniques. The first substance to be investigated was calcite ( $\text{CaCO}_3$ ) containing manganese as a paramagnetic impurity. Although the x-rays produced a strong luminescence in the calcite, it turned out that the agency responsible for the effect either does not involve free electrons and consequently is not paramagnetic, or the temperature at which the experiment was performed is not low enough.

With the facilities at hand, it was decided to carry out research in crystals of symmetry lower than cubic. This is because very little work has been done in this class of substances and if the impurities happen to be of the iron transition group with long time constants ( $\text{Fe}^{+3}$ ,  $\text{Mn}^{+2}$ ,  $\text{Cr}^{+3}$ , etc.)

the experiment could be performed at temperatures higher than that of liquid helium.

The measurement of the g-factor and the zero field splitting constants would indicate the order of admixture of the higher excited states of the paramagnetic ion for the sites of such low symmetry. The class of substances that were selected for study were the pyroxenes and in particular spodumene ( $\text{LiAl}(\text{SiO}_3)_2$ ). Samples of spodumene at hand contained a large number of impurities of which iron occurred in the greatest concentration.

## II

### THEORY

The general Hamiltonian of a free ion placed in an external magnetic field is given by

$$H = V_F + V_{LS} + V_{SS} + V_N + V_Q + V_H + V_{NH} \quad (1)$$

When the free ion is placed in a crystalline field, we must include the electrostatic interaction term,  $eV_C$ . This accounts for the interaction of the free ion with the electric field of the neighbouring ions. The dipole-dipole interaction between the nuclear moment and the magnetic moments of the electrons  $V_N$ , the interaction of the quadrupole moment  $Q$  of the nucleus with the electrostatic field gradient  $V_Q$ , and the interaction of the external magnetic field  $H$  with the nucleus,  $V_{NH}$  are all zero. This is because the paramagnetic ion of iron  $Fe^{+3}$  has no nuclear magnetic moment. Also we shall not consider the spin-spin interaction  $V_{SS}$  at this time. Therefore the resultant Hamiltonian is

$$H = V_F + V_{LS} + V_H + V_C \quad (2)$$

Here  $V_F$  is the coulomb interaction between the nucleus and its surrounding electrons. It has the form:

$$V_F = \sum_{k=1}^N \left\{ p_k^2 / 2m - Ze^2 / r_k \right\} + \sum_{k>j=1}^N e^2 / r_{kj} \quad (3)$$

Here  $p_k$  is the linear momentum of the  $k$ th electron and  $r_k$



is the magnitude of the positional vector from the center of the nucleus to the  $k$ th electron. The running index  $k$  includes all of the electrons of the ion and  $j$  is always different from  $k$  but they both represent electrons. This interaction usually has the approximate magnitude  $10^5 \text{ cm}^{-1}$ .

The second most important interaction is the spin-orbit coupling  $V_{LS}$  between the spin and orbital momentum of the electron. If we consider only states of definite  $L$  and  $S$ , the spin-orbit interaction can be written as

$$(4) \quad V_{LS} = \lambda \vec{L} \cdot \vec{S} \text{ where } \lambda \text{ is the spin-orbit constant for a given ion. Also } \vec{L} \text{ and } \vec{S} \text{ can be written as}$$

$$\vec{L} = \sum_{k=1}^N \vec{l}_k \quad \vec{S} = \sum_{k=1}^N \vec{s}_k \quad (5)$$

The crystalline field is regarded as a system of point or dipole charges surrounding the paramagnetic ion. This supposedly sets up a static field which acts on the paramagnetic ion and changes the electronic orbits. Usually perturbation theory is used to calculate the effect of the crystalline field. The crystalline field has been found experimentally to fall into three types. Firstly there is the strong field interaction, wherein  $V_C$  is of the order of the energy caused by the electron repulsion term ( $10^4 \text{ cm}^{-1}$ ). Secondly there is the medium field interaction in which the energy intervals are of the same order as those of the multiplets of the same electron configuration. Here perturbation theory is applied before calculating  $V_{LS}$ . Thirdly we have the weak field interaction, wherein the energy intervals caused by the crystalline field are very small compar-

ed to the spin-orbit energy level differences. The three degrees of interaction are defined with respect to the relative magnitude of the other terms of the Hamiltonian. The point at which the crystalline field will be used as a perturbation calculation depends on this relative magnitude consideration.

If we regard the point charges, as not overlapping the paramagnetic ion, the electrostatic potential is then a solution of Laplace's equation

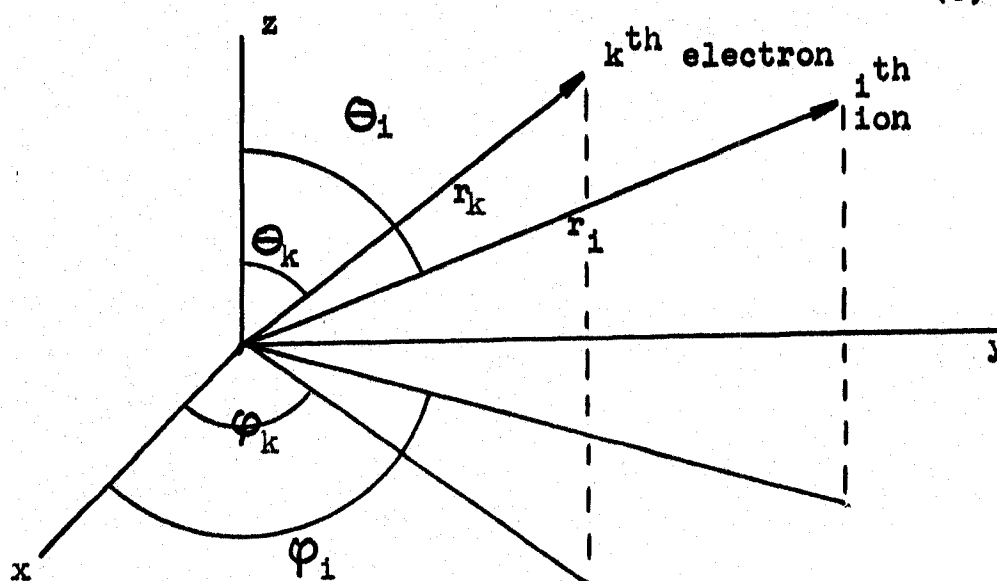
$$\nabla^2 V = 0 \quad (6)$$

The generalized Legendre polynomials are solutions of this equation. The potential can be written in the following form:

$$V = \sum_n \sum_{m=-n}^n \sum_k A_n^m r^n Y_n^m(\theta_k, \phi_k) \quad (7)$$

Here  $k$  is summed over all the electrons and the normalized harmonics  $Y_n^m$  are defined as

$$Y_n^m(\theta_k, \phi_k) = (-1)^n \left\{ \frac{1}{4\pi} \frac{(2n+1)(n-|m|)!}{(n+|m|)!} \right\}^{1/2} P_n^m(\cos \theta) e^{im\phi_k} \quad (8)$$



The wavefunctions of the electrons can be expressed in harmonic functions ( $\psi_l^i \sim R(r_l) Y_l^i(\theta_l, \phi_l)$ ) where  $R(r_l)$  refers to the radial part of the wavefunction. Since the matrix elements are of the form  $\psi_l^i V_m^m \psi_l^i$  where

$$V_m^m = \sum_{\kappa} A_{\kappa}^m r^{\kappa} Y_{\kappa}^m(\theta_{\kappa}, \phi_{\kappa}) \quad (9)$$

then the matrix elements for  $n > 2l$  are zero. Also all terms with odd  $n$  must vanish. This is because the product  $\psi_l^i \psi_l^i$  is unchanged by inversion symmetry, whereas the odd rank terms of the potential change sign. Even if there is no center of symmetry the odd terms are still zero but there now may be terms from the admixture of higher levels. The term  $n = 0$  only adds a constant to the expansion and adds nothing of significance. Since we are concerned with  $d$  electrons, we need only consider the values, 2 and 4 for  $n$ . Therefore

$$\begin{aligned} V &= \sum_{m=\pm 2} \sum_{\kappa} A_{\kappa}^m r^{\kappa} Y_{\kappa}^m + \sum_{m=\pm 0, \pm 1, \pm 2} \sum_{\kappa} A_{\kappa}^m r^{\kappa} Y_{\kappa}^m \\ &= \sum_{\kappa} A_{\kappa}^0 r^{\kappa} Y_{\kappa}^0 + \sum_{\kappa} A_{\kappa}^2 r^{\kappa} Y_{\kappa}^2 + \sum_{\kappa} A_{\kappa}^{-2} r^{\kappa} Y_{\kappa}^{-2} + \sum_{\kappa} A_{\kappa}^0 r^{\kappa} Y_{\kappa}^0 + \sum_{\kappa} A_{\kappa}^4 r^{\kappa} Y_{\kappa}^4 \\ &+ \sum_{\kappa} A_{\kappa}^{-4} r^{\kappa} Y_{\kappa}^{-4} + \sum_{\kappa} A_{\kappa}^2 r^{\kappa} Y_{\kappa}^2 + \sum_{\kappa} A_{\kappa}^{-2} r^{\kappa} Y_{\kappa}^{-2} + \sum_{\kappa} A_{\kappa}^3 r^{\kappa} Y_{\kappa}^3 \\ &+ \sum_{\kappa} A_{\kappa}^{-3} r^{\kappa} Y_{\kappa}^{-3} + \sum_{\kappa} A_{\kappa}^4 r^{\kappa} Y_{\kappa}^4 + \sum_{\kappa} A_{\kappa}^{-4} r^{\kappa} Y_{\kappa}^{-4} \quad (10) \end{aligned}$$

Let us now consider a particular symmetry for the crystalline field. For spodumene we shall assume that it has sixfold tetragonal co-ordination. The symmetry in this case removes a number of terms from the potential. This is

because the paramagnetic ion involved sees the same physical situation for different orientations. In this case, it is for rotations of ninety degrees about the tetragonal axis. For example, if we consider the rhombic component of the crystalline field and perform an operation of rotation by ninety degrees, the crystalline potential must be the same. Therefore we can write:

$$V_R = \sum A_2^0 r^2 y_z^2 + \sum A_2^{\pm 2} r^2 y_z^{\pm 2} + \sum A_4^0 r^4 y_z^4 + \sum A_4^{\pm 2} r^4 y_z^{\pm 2} \quad (11)$$

Here  $A_n^m = \text{const. } P_n^m \cos \theta_1 (e^{im\phi_1})$

Now  $V_R = C_4 \cdot V_R$ . Here only the A's are operated upon by the  $C_4$  operator. Under the  $C_4$  operation only the  $\phi_1$  dependence is involved. Now we have

$$C_4 A_n^m = \text{const. } e^{im\phi_1} \cdot e^{im\pi/2} \quad (12)$$

$$\therefore C_4 A_n^{\pm 2} = -A_n^{\pm 2} \text{ but } A_n^{\pm 2} = C_4 A_n^{\pm 2}$$

$$\therefore A_n^{\pm 2} = -A_n^{\pm 2} = 0.$$

Also we do this for the axial, tetrahedral and the remaining terms of the crystalline potential and we obtain the final form of the crystalline potential. It is

$$V = \sum A_2^0 r^2 y_z^2 + \sum A_4^0 r^4 y_z^4 + \sum A_4^{\pm 4} r^4 y_z^{\pm 4} + \sum A_4^{\pm 2} r^4 y_z^{\pm 2} \quad (13)$$

Equation (13) can also be written with respect to the distances between the neighbouring ions, as shown in Fig. 1' and has the form:

$$V = C_2 \left\{ 2 \left[ \frac{1}{a_1^3} + \frac{1}{a_2^3} \right] y_z^2 \right\} + C_4 \left\{ \frac{1}{2} \left[ \frac{4}{a_1^5} + \frac{3}{a_2^5} \right] y_z^4 \right. \\ \left. + \frac{1}{4} a_2^5 \{ 70 \}^{1/2} (y_4^4 + y_4^{-4}) \right\} \quad (14)$$

where

$$C_2 = \frac{Z_i e^2 r^2}{a_i^3} \left\{ \frac{4\pi}{13} \right\}^{1/2}$$

$$C_4 = \frac{Z_i e^2 r^4}{a_i^5} \left\{ \frac{4\pi}{9} \right\}^{1/2}$$

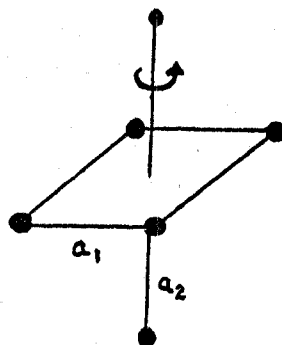


Fig. 1'

Also it can be written in cartesian co-ordinates as

$$V = C_4(x^4 + y^4 + z^4 - 3/5 r^4) + A_2^0(x^2 + y^2 - 2z^2) + A_4^0(35z^4 - 30r^2 z^2 + 3r^4) + A_4^4(x^4 - 6x^2 y^2 + y^4) \quad (15)$$

Now if we want the perturbation due to the crystalline field on the energy levels, involving the matrix elements between the magnetic sublevels of the spin, then the method of equivalent operators is used. This method was developed by Stevens (1952), Elliott (1953) and by Judd (1955). To use it, one replaces each  $x$ ,  $y$  and  $z$  by the equivalent operators  $S_x$ ,  $S_y$ , and  $S_z$  which are the spin momentum operators for the manifolds of constant  $S$ . One must have the proper regard for the commutation rules of these operators. In our case, the matrix elements are given by

$$\begin{aligned} \langle M_S | V | M_S' \rangle &= C_4 \langle M_S | \frac{B F^4}{20} \{ 35 S_z^4 - 30 S(S+1) S_z^2 + 25 S_z^2 - 6 S(S+1) + 3 S^2(S+1)^2 \} | M_S' \rangle \\ &+ C_4 \langle M_S | \frac{B F^4}{5} \{ S_+^4 + S_-^4 \} | M_S' \rangle + A_2^0 \langle M_S | \alpha \bar{r}^2 (3 S_z^2 - S(S+1)) | M_S' \rangle \\ &+ A_4^0 \langle M_S | \frac{B F^4}{5} \{ 35 S_z^4 - 30 S(S+1) S_z^2 + 25 S_z^2 - 6 S(S+1) + 3 S^2(S+1)^2 \} | M_S' \rangle \\ &+ A_4^4 \langle M_S | \frac{1}{2} B F^4 \{ S_+^4 + S_-^4 \} | M_S' \rangle \end{aligned} \quad (16)$$

Therefore the addition of the crystalline field potential to the Hamiltonian is  $V = C_4 \frac{B_4}{20} \{ 35 S_z^4 - 30 S(S+1) S_z^2 + 25 S_z^2 -$

$$6 S(S+1) + 3 S^2(S+1)^2 \} + C_4 \frac{B_4}{20} \{ S_+^4 + S_-^4 \} + A_2^0 \alpha r^2 \{ 3 S_z^2 - S(S+1) \} + A_4^0 B_4^{-1} \{ 35 S_z^4 - 30 S(S+1) S_z^2 + 25 S_z^2 - 6 S(S+1) + 3 S^2(S+1)^2 \} + A_4^4 \frac{1}{2} B_4^{-1} \{ S_+^4 + S_-^4 \}$$

(17)

where

$$\beta = \mp \frac{3(2l+1-4s) - 7(l-2s)(l-2s+1) + 3(l-1)(l+2)}{(2l-3)(2l-1)(2l+3)(2l+5)(l-1)(2l-3)} : \alpha = \mp \frac{2(2l+1-4s)}{(2l-1)(2l+3)(2l-1)}$$

and where the minus sign is used for less than half filled shells and where the plus sign is used for more than half filled shells. The above matrix elements for the crystalline field are usually found in tables (Low 1960).

To see in a qualitative way how the ground state of an ion splits in a crystalline field, we can use group theoretical methods. This method does not predict the order in which the levels lie or the separation between them. We must determine the matrix elements above for this information. Here we will only state the results of the group theoretical method for the paramagnetic ion  $Fe^{+3}$  whose ground state is  $^6S$ . The complete results of the group theoretical treatment have been worked out by Bethe (1929) and they are listed by Low (1960)

For the case of  $Fe^{+3}$  we consider the spin-orbit coupling to be much stronger than the crystalline field effect. The ground state of  $Fe^{+3}$  is  $^6S_{5/2}$ . First we consider the symmetry of the closest neighbours to be cubic. This results in the appearance of the crystal field levels whose symmet-

ries are  $\Gamma_7$  and  $\Gamma_8$  of the cubic irreducible representation (See Table XV of Low 1960). These splittings are shown in Fig. 2.

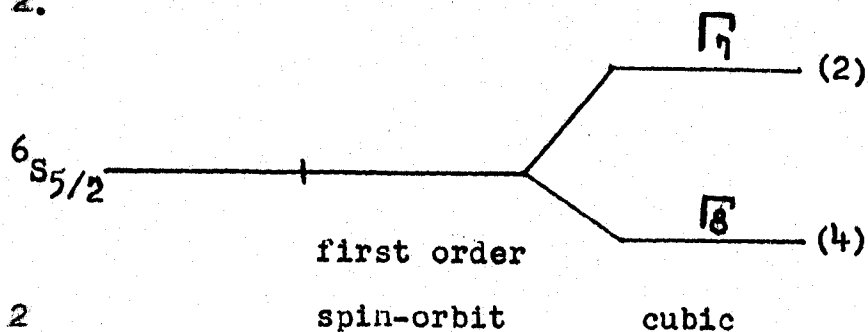


Fig. 2

Here we have the ground state split into two levels,  $\Gamma_7$  and  $\Gamma_8$ . The  $\Gamma_7$  level is twofold degenerate and the  $\Gamma_8$  is fourfold degenerate. Now if we consider a tetragonal component belonging to the crystal field symmetry, the levels that were created by the cubic field symmetry split. We now have (according to Table XVI of Low 1960) the  $\Gamma_7$  level going over into a  $\Gamma_{t7}$  and the  $\Gamma_8$  level going over into a  $\Gamma_{t6}$  and a  $\Gamma_{t7}$ . This is shown in Fig. 3.

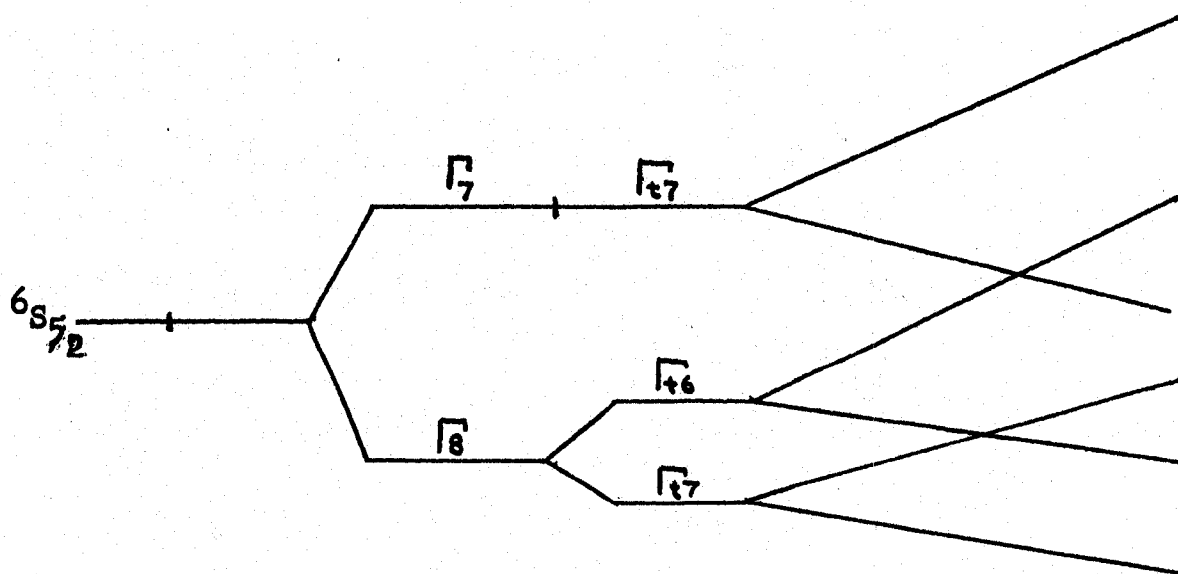


Fig. 3 spin-orbit cubic tetragonal magnetic field

We see that  $\Gamma_7$  remains a twofold degenerate level, whereas  $\Gamma_8$  splits into new levels which are both twofold degenerate,  $\Gamma_{t6}$  and  $\Gamma_{t7}$ . If we apply a steady magnetic field as shown in Fig. 3, the degeneracy is completely removed.

Let us now return to the Hamiltonian, which is

$$H = V_F + V_{LS} + V_H + eV_C \quad (18)$$

Consider only the perturbation part:

$$H = V_H + eV_C \quad (19)$$

In paramagnetic resonance only transitions between the lowest energy levels are observed. These levels between which transitions occur could be treated as isolated levels and the higher lying levels ignored. If in the case of the free ion, a state of quantum number  $S$  splits into  $2S + 1$  levels in an external magnetic field and if only transitions between  $2S' + 1$  levels are observed experimentally, then  $S'$  can be defined as the fictitious spin of the system. Let us now drop the prime on  $S'$ . Therefore the spin Hamiltonian can be written:

$$H_S = \beta \vec{H} \cdot \vec{g} \cdot \vec{S} + eV_C \quad (20)$$

Here  $\beta$  is the Bohr magneton and  $g$ , a tensor, is the spectroscopic  $g$ -factor. In our case we have axial symmetry and we can write the spin Hamiltonian as

$$H_S = g_{||} \beta H_z S_z + g_{\perp} \beta (H_x S_x + H_y S_y) + eV_C \quad (21)$$

Here  $g_{||}$  is along the symmetry axis and  $g_{\perp}$  is normal to the symmetry axis. Let us transform the Hamiltonian, by a rotation of the axes to a simple  $g\beta H S_z'$ . Consider the transformed



axes having the Euler angles  $(\psi', \delta', \varphi')$  with respect to the coordinate system of the crystal field. Also the magnetic field makes the angles  $(\Theta, \delta, \varphi)$  with respect to the crystal-line field. The transformation of the general Zeeman term,  $g_x S_x H_x + g_y S_y H_y + g_z S_z H_z$ , is carried out in Low 1960. The transformation equations for the magnetic field components are

$$\begin{aligned} H_x &= H \sin \Theta \sin \delta \\ H_y &= -H \sin \Theta \cos \delta \\ H_z &= H \cos \Theta \end{aligned} \quad (22)$$

The transformation equations for the spin components are

$$\begin{aligned} S_z &= -ab S_+^1 + (aa^* - bb^*) S_z^1 - a^* b^* S_-^1 \\ S_+ &= a^2 S_+^1 + 2a b^* S_z^1 - b^{*2} S_-^1 \\ S_- &= a^{*2} S_-^1 + 2a^* b S_z^1 - b^2 S_+^1 \end{aligned} \quad (23)$$

Therefore the Zeeman term becomes

$$\begin{aligned} &S_z^1 (1/2(g_x - g_y)(ab^* H_+ + a^* b H_-) + 1/2(g_x + g_y)(ab^* H_- + a^* b H_+)) + (aa^* - bb^*) g_z H_z + S_+^1 (1/4(g_x - g_y)a^2 H_+ + 1/4(g_x + g_y)(a^2 H_- - b^2 H_+) - ab g_z H_z) + S_-^1 (1/4(g_x - g_y)(a^{*2} H_- - b^{*2} H_+) + 1/4(g_x + g_y)(a^{*2} H_+ - b^{*2} H_-) - a^* b^* g_z H_z) - S_+^1 b^2 H_- \end{aligned} \quad (24)$$

where  $H_{\pm} = H_x \pm i H_y$ ,  $a = \cos \frac{1}{2} \Theta e^{\frac{i}{2}(\delta' + \varphi')}$ ,  $b = i \sin \frac{1}{2} \Theta e^{\frac{i}{2}(\delta' + \varphi')}$

If we only want the diagonal terms, the coefficients of  $S_+^1$  and  $S_-^1$  must be zero. This leads to

$$\begin{aligned} \sin \psi' &= (g_{\perp}/g) \sin \Theta & g_{\perp}^2 &= g_x \sin^2 \delta + g_y^2 \cos^2 \delta \\ \cos \psi' &= (g_{\parallel}/g) \cos \Theta & g^2 &= g^2 \cos^2 \Theta + g^2 \sin^2 \Theta \\ \sin \delta' &= (g_x/g_{\perp}) \sin \delta & g_{\parallel} &= g_z \\ \cos \delta' &= (g_y/g_{\perp}) \cos \delta \end{aligned} \quad (25)$$

Since there is axial symmetry present, the following three relations are valid

$$\delta = \delta' , \quad \varphi = \varphi' \quad g_x = g_y \quad (26)$$

The variation (angular) in the g-factor is, as a result of equation (26)

$$\begin{aligned} \text{and} \quad g^2 &= g_{\parallel}^2 \cos^2 \theta + g_{\perp}^2 \sin^2 \theta \\ g_{\perp} &= \text{const.} \end{aligned} \quad (27)$$

If a spectrum is taken such that the external magnetic field rotates in a plane normal to the symmetry axis, then by equation (27) we have  $\theta = \pi/2$  and  $g = g_{\perp}$ . Further if a spectrum is taken with the external magnetic field direction along the symmetry axis, then by equation (27) we have  $\theta = 0$  and  $g = g_{\parallel}$ . Both of these situations were included in the experiment and the results are set forth in chapter four. We have neglected the crystalline field term.

### III

#### APPARATUS

The electron-spin resonance spectrometer used was a superheterodyne type, as described by Low (1961) and Feher (1956). The spectrometer operates at a 3.3 centimeter wavelength and employs a 30 megacycle intermediate frequency. The block diagram of the spectrometer is shown in Fig. 1.

In order to explain the function of the component parts of the spectrometer, it is convenient to consider the entire system to be divided into three parts: (1) the signal microwave components, (2) the signal detection and amplification system, and (3) the frequency control system.

##### 1. The Signal Microwave Components

The power from the signal klystron, whose direction is indicated by the arrow of the ferrite isolator, enters the E-arm of the magic tee,  $T_1$ . Half of the microwave power is transmitted down each side arm of the magic tee. There is connected to one side arm a slide-screw tuner and a resonant cavity, and to the other side arm there is attached a phase shifter, an attenuator and a line termination. These elements, the phase shifter, the attenuator, the slide-screw tuner, the characteristic impedance of the line and the cavity, can be considered as components of a radio-frequency

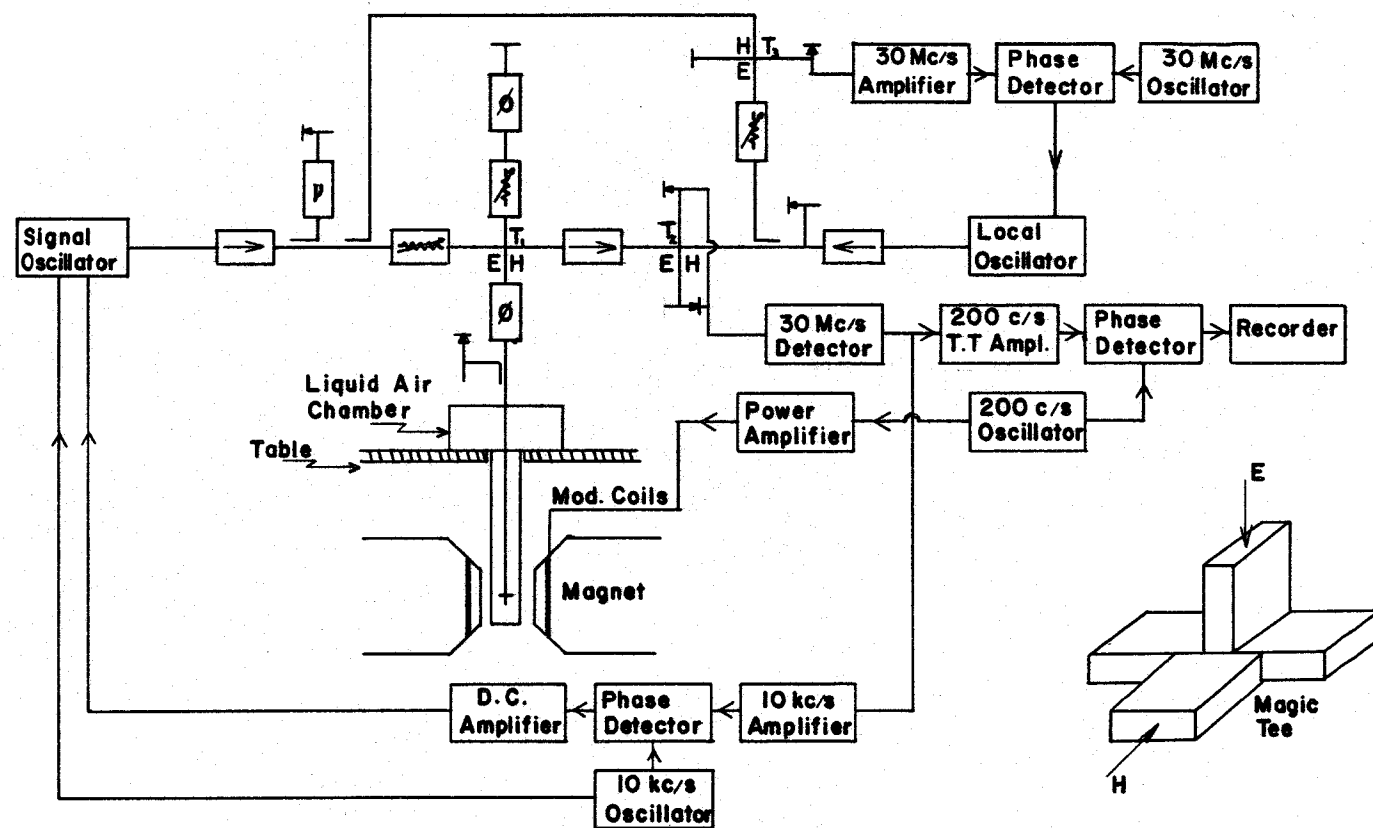
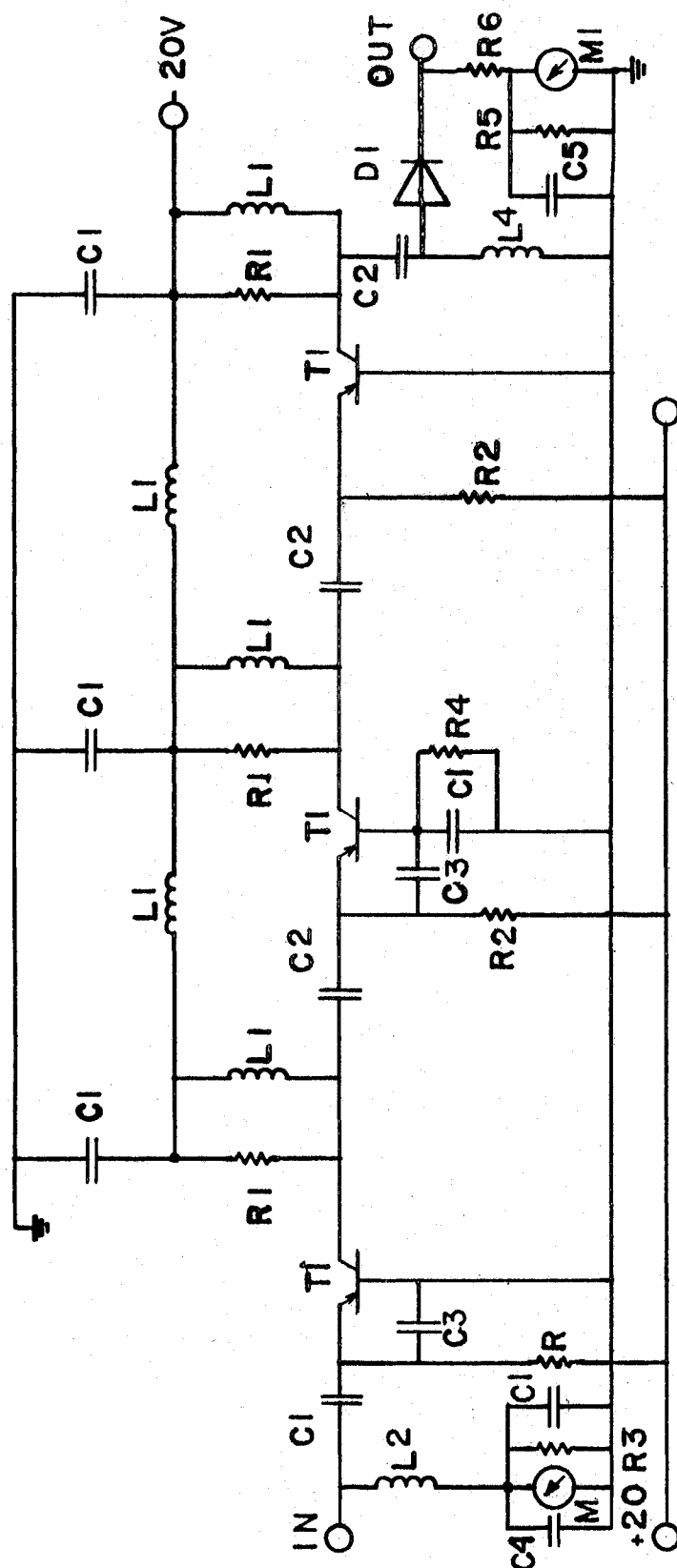


Fig 1. Superheterodyne Paramagnetic Spectrometer

bridge and serve to tune out any reflected power that appears in the H-arm. At resonance, the bridge becomes unbalanced and consequently microwave power appears in the H-arm and is transmitted via the ferrite isolator to the E-arm of the magic tee,  $T_2$ . The above isolator serves to attenuate any power reflected from  $T_2$ , which might appear in the H-arm of the cavity bridge and thus unbalance it. The magic tee,  $T_2$ , is essentially a balanced mixer. A pair of matched reversed diode detectors constitute the side arms of this bridge, while the H-arm serves to introduce the local oscillator power, whose frequency is held accurately at 30 megacycles above (or below) that of the signal oscillator. The power from both the signal oscillator and the local oscillator divides equally between the side arms. The power of the local oscillator divides in phase and that of the signal oscillator out of phase. But since the diodes are reversed, the signal power only appears at the output of the mixer. This arrangement ensures a high conversion gain and the cancellation of any noise from the local oscillator appearing in the detection system.

## 2. The Signal Detection And Amplification System

The signal from the crystal mixer is fed into a 30 megacycle amplifier and detector. Its circuit diagram is given in Fig. 2. The detector is a 1N34 diode. The signal appearing at the output of the 1N34 diode is fed into both a 200 c/s amplifier and a 10 kc/s amplifier. The



T1	2N502	C4	0.001uf	R3	56	M	0-1 ma
C1	0.01uf	C5	0.05 uf	R4	10K	M1	50-0-50ua
C2	20 uf	R1	4.7K	R5	68	D1	IN34 Diode
C3	220 uf	R2	6.8K	R6	10K	L1, L2, L3	R.F.C.
							Tuned to 30Mc.

Fig. 2 30Mc/s Amplifier and Detector

10 kc/s amplifier is part of the frequency control system and is described below. The 200 c/s amplifier, as shown in Fig. 3, is a narrow bandwidth amplifier and is tuned for 200 c/s by means of the twin-tee network. From the 200 c/s amplifier, the signal is fed into a lock-in detector. Its circuit is shown in Fig. 4. This signal from the 200 c/s amplifier has a frequency of 200 c/s and it must have the same phase as the 200 c/s reference signal mentioned below. The reference signal is also a 200 c/s signal of fixed amplitude, that is provided by the same 200 c/s oscillator that supplies power to the modulation coils. The function of the phase detector is to convert the 200 c/s signal in the two 1N34 diode rectifier systems into a d-c. voltage. The polarity of the d-c. voltage depends on the phase relationship of the signal input to the reference input. Finally, the d-c. signal of the phase detector is recorded on a Varian Associates strip recorder.

### 3. The Frequency Control System

There are two frequency control loops; one regulates the frequency of the signal oscillator and one regulates the frequency of the local oscillator.

Referring to Fig. 1, it can be seen that a fraction of the power of each oscillator is sampled out by directional couplers, and one is fed into the E-arm and one is fed into the H-arm of the magic tee,  $T_3$ . The two signals are mixed

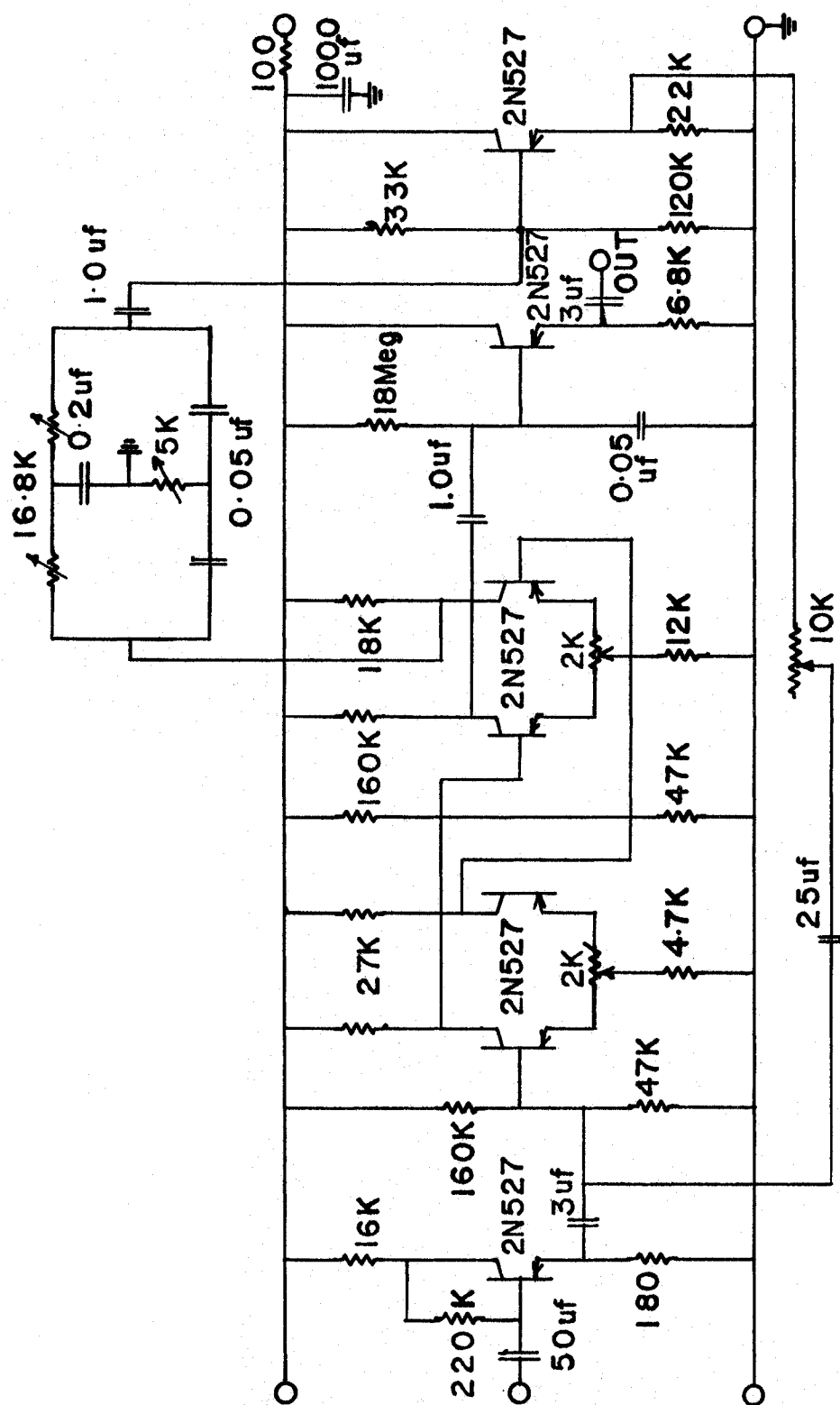


**Fig. 3** 200 c/s Amplifier



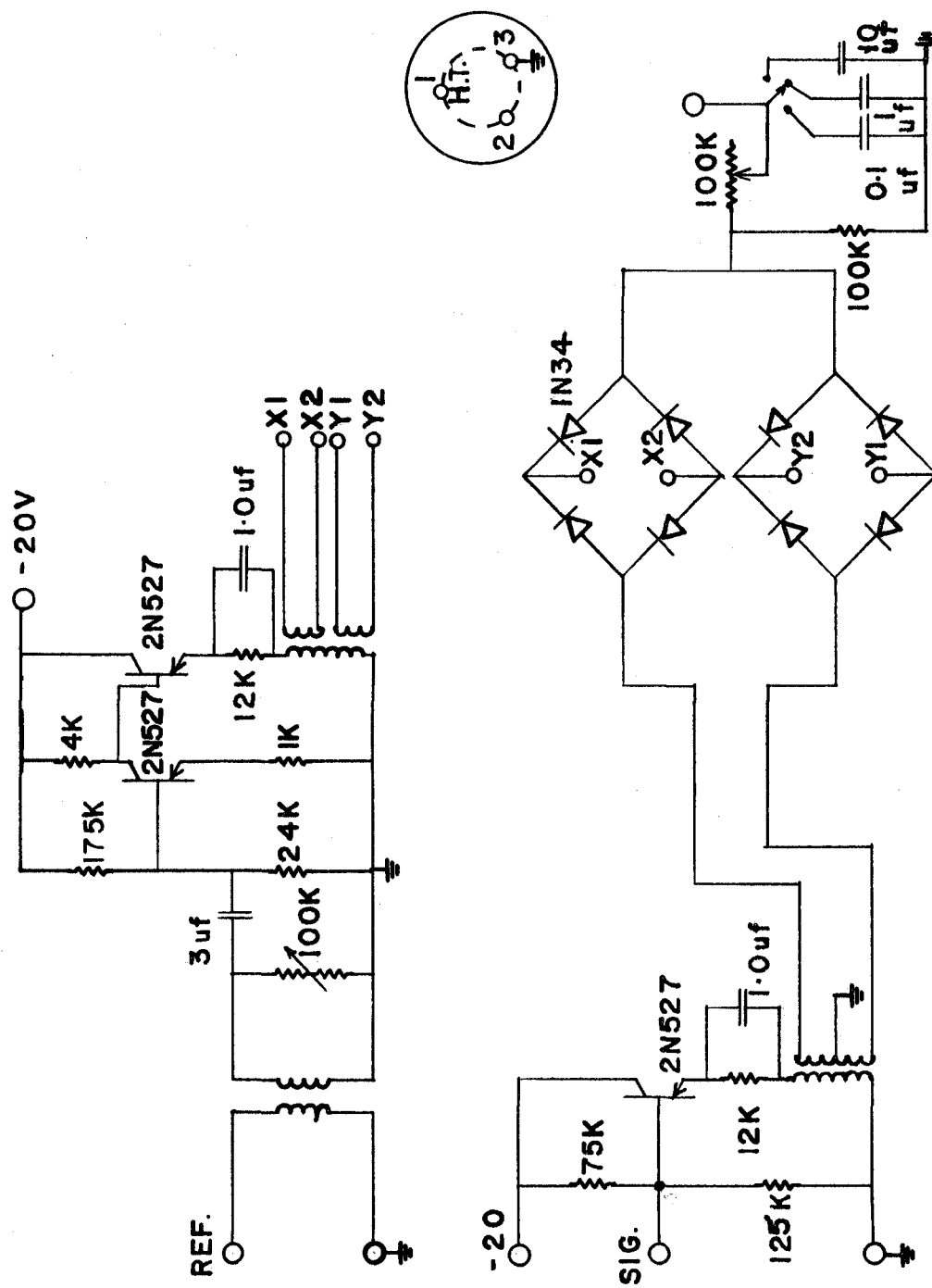


Fig. 4 Lock-in Detector

in the diode which is attached to one side arm of the magic tee, while the other side arm is terminated by its characteristic impedance. The beat signal appearing at the output of the crystal detector is fed into a 30 Mc/s tuned amplifier. The circuit of the amplifier is shown in Fig. 5. The amplified beat signal is then fed into a phase detector and compared to a 30 Mc/s signal provided by a crystal controlled oscillator. Fig. 6 gives the circuit of the phase detector. The phase relationship between the signal and the reference waveforms determines the polarity of the d-c. signal returned to the reflector of the local oscillator. The polarity of this signal determines the direction of the shift in the frequency of the local oscillator. By this means, the local oscillator is kept 30 Mc/s above (or below) the signal klystron frequency.

The stabilization of the signal klystron is accomplished in the following manner. The reflector of the signal klystron is modulated by a very small 10 kc/s signal. Suppose that the signal klystron is tuned to the frequency of the sample cavity, then any tendency of the klystron to drift results in an error signal at the modulation frequency appearing at the output of the balanced mixer. Consequently the reflected power from the cavity is modulated by the 10 kc/s and is detected in the same manner as the resonance signal. The signal appearing at the 1N34 diode of the 30 megacycle amplifier and detector is fed into the 10 kc/s amplifier. The 10 kc/s amplifier is shown in Fig. 7. The error signal from the 10 kc/s amplifier

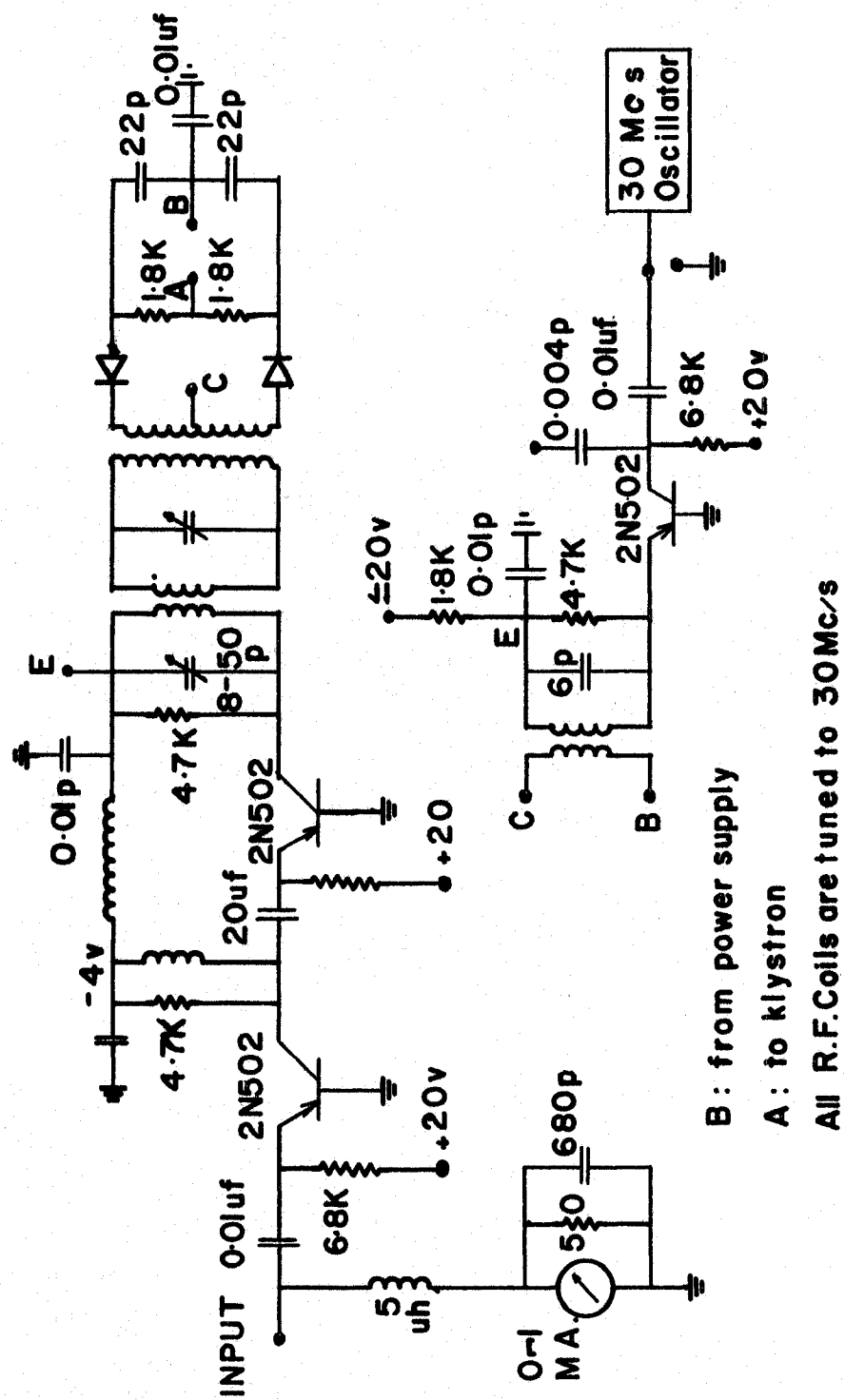


Fig. 5 & 6 30Mc/s Amplifier and Phase Detector

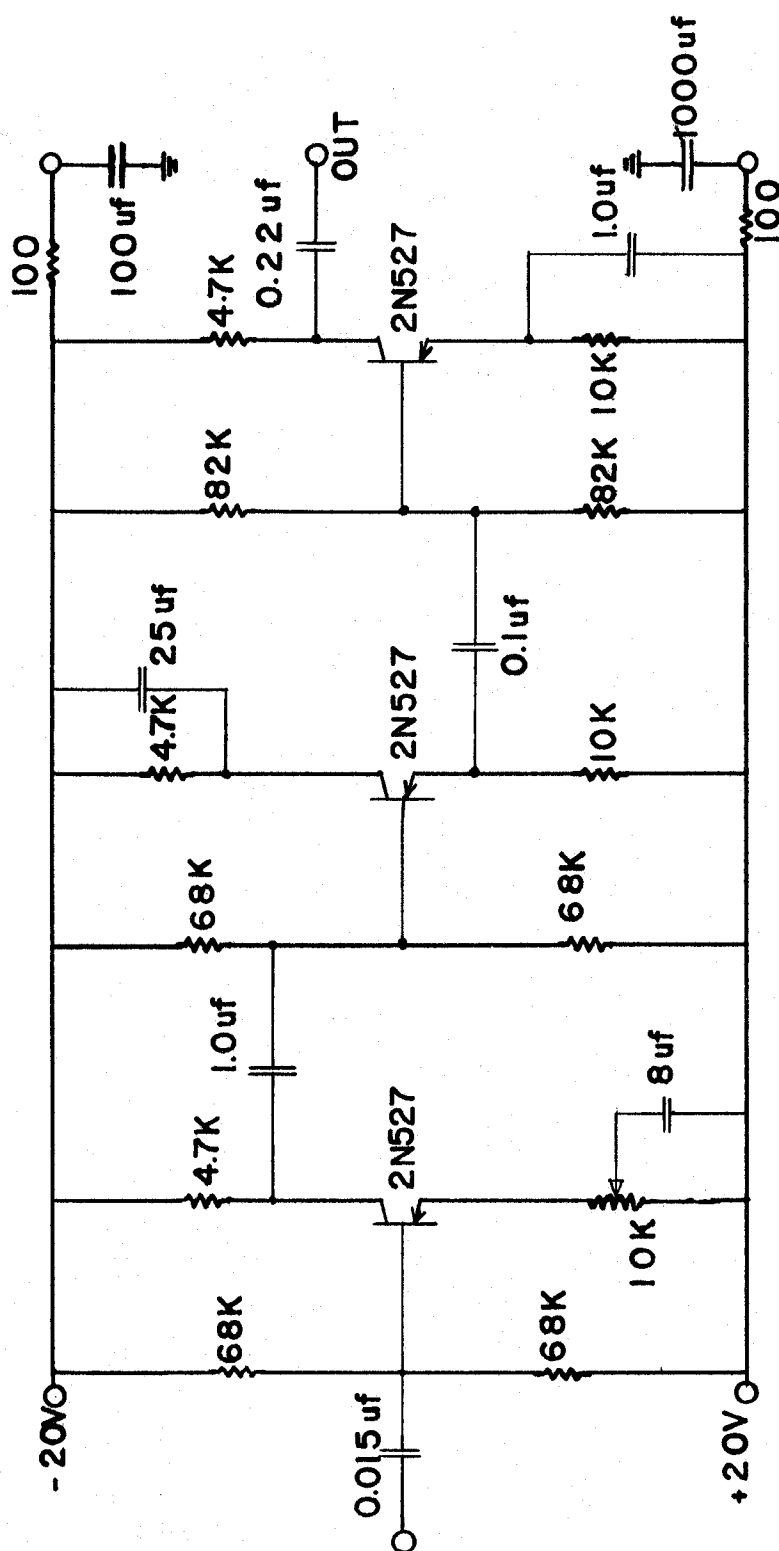


Fig. 7 10k/c Amplifier

enters the input end of the phase detector. Fig. 8 gives the circuit diagram of the phase detector. Both the reference frequency and the modulation frequency for the signal klystron is provided by the same generator, as shown in Fig. 9. The d-c. output voltage of the 1N34 diode rectifiers is amplified by a directly coupled difference amplifier and is fed back to the reflector of the signal klystron. If the polarity of the d-c. error signal is of the proper sign then any tendency for the frequency of the signal klystron to drift is compensated.

In addition to the components described, the electron-spin resonance spectrometer has a few other measuring devices. There is a wavemeter next to the signal klystron for the purpose of measuring the resonant frequency of the cavity. Provision is also made to view the cavity by means of a directional coupler and a crystal detector. At the local oscillator output there is provided a crystal detector to view the mode of oscillation of the klystron so that it can be centered about the signal klystron frequency.

The particular klystrons used, the electromagnet, its power supply, the N.M.R. probe, the cryostat and the associated vacuum system, the cavities, and the operation of the spectrometer are now described.

The microwave power sources were two Varian 203/675 reflex klystrons rated at a power level of 50 milliwatts. They are water cooled and tunable over the range from

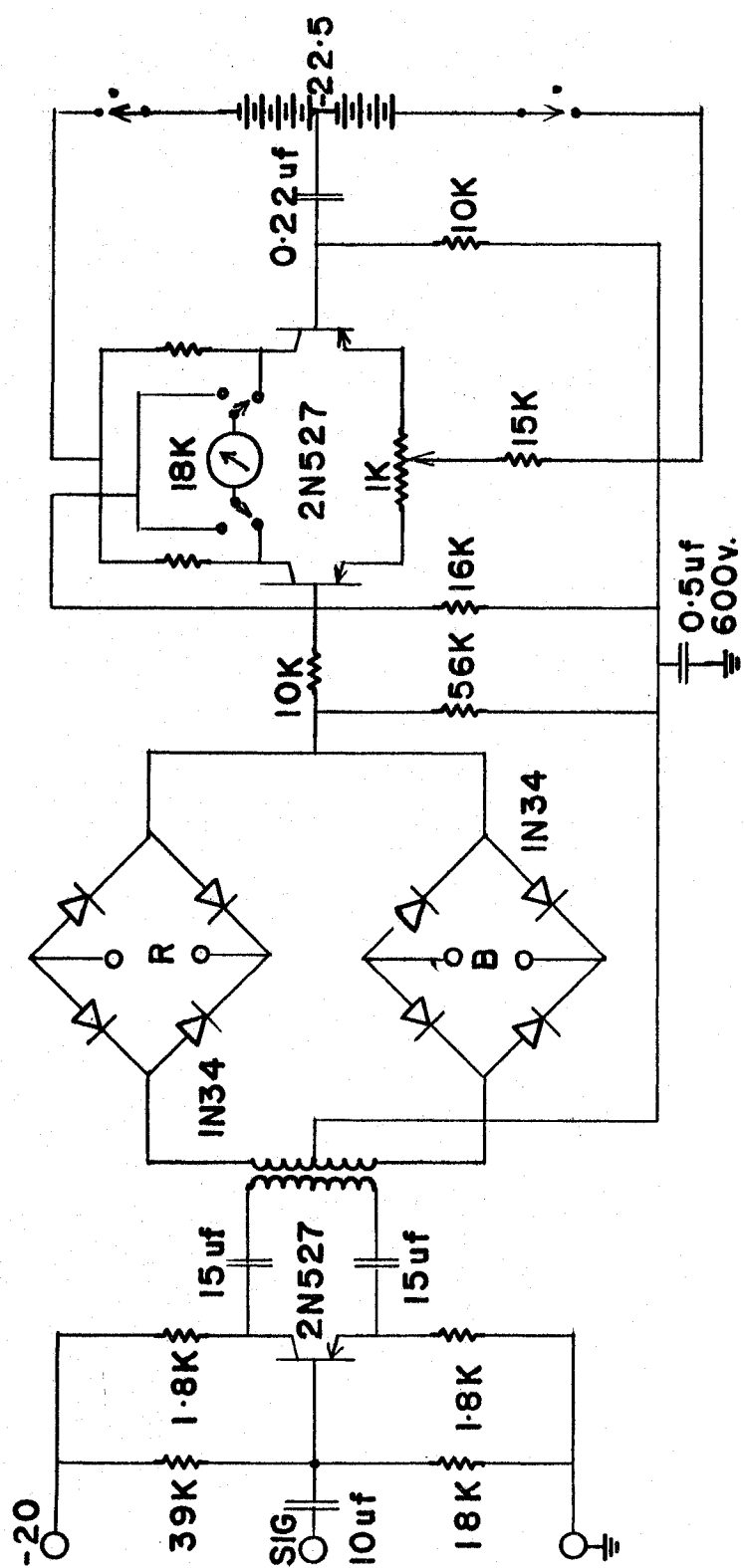


Fig. 8 Phase Detector



8.5 Gc/s to 9.6 Gc/s. The beam current used was approximately 30 milliamperes and it was supplied by a Lambda regulated power supply, model 25. Six volt storage batteries supplied the 0.4 - 0.5 amperes heater currents. The voltage on the reflectors of the klystrons was provided by a shielded battery bank of various sized dry cells. The battery bank for the reflex klystron is shown in Fig. 10. The voltage on the reflectors can be increased or decreased in steps of 22.5 volts or 3 volts, from a fixed voltage of -337.5 volts or -37.5 volts with respect to the ground or to the cathode, respectively. Also on the battery banks there is supplied a voltage that can be varied continuously over a 4.5 voltage range for a particular step voltage setting.

The magnet used was a Newport 7" electromagnet, type E. The gap between the pole faces is adjustable and the poles carry universal screw shims. We used a gap width of 6 centimeters and a magnetic field range of 0.5 kilogauss to 5 kilogauss. The universal screw shims were set approximately 0.16 centimeters out from the pole faces to ensure a better homogeneity in the magnetic field. The magnetic field variation over the paramagnetic specimen was no more than one gauss in  $10^3$  gauss for a field of 5 kilogauss. The stability of the magnet power supply as quoted by the manufacturer was one part in  $10^4$  on the low current range (0.5 - 12 amp.) for a mains input variation not exceeding 4%. The field ripple was 0.5 gauss, peak to peak. We varied the steady field by applying a continuously increasing



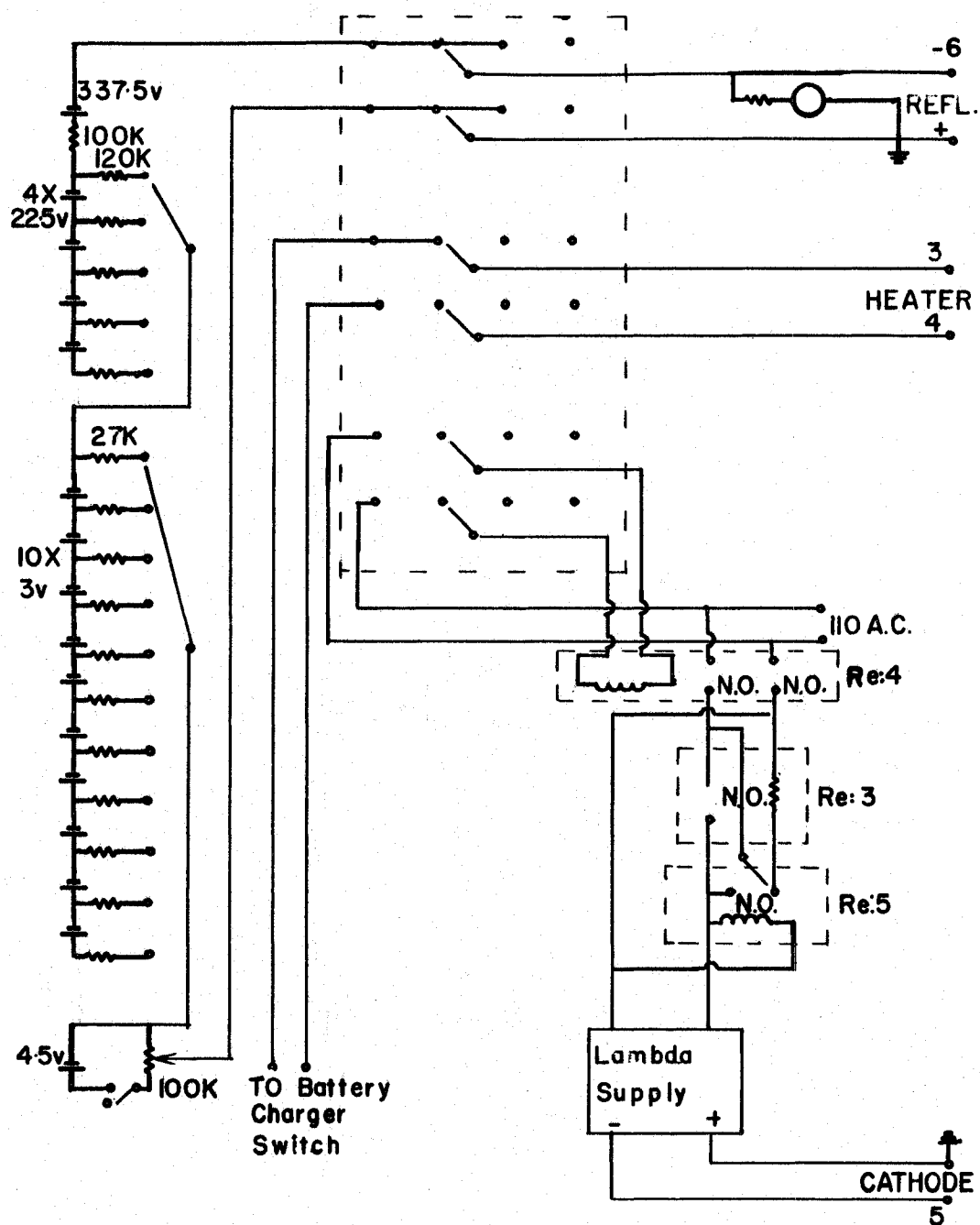


Fig 10 KLYSTRON POWER SUPPLY

electromotive force to the sweep input of the power supply. This was done by tapping the voltage across a rheostat by means of a synchronous motor driven slide wire. The sweep rate was approximately 2.5 gauss/sec. The steady magnetic field modulation is provided by coils wound in the same plane as that of the pole faces of the magnet. They are mounted side by side with the coils of the steady magnetic field. The modulation coils are powered by a 200 c/s oscillator, as shown in Fig. 11, driving a power amplifier, Fig. 12, and they provided a modulation field of 10 gauss.

To measure the steady magnetic field we used a proton resonance probe. The sample was held in a 7 mm. diameter tube. It (the sample) was water with a small amount of copper sulfate or ferric nitrate in order to shorten the relaxation time of the resonance line. It is the proton of hydrogen in the water which is responsible for the resonance line. The probe proper consists of a calibrated marginal oscillator and a detector amplifier system. The modulation coils of the probe were supplied with the output of the 60 c/s sweep circuit whose maximum output was three volts peak to peak. Since the tunable frequency range of the oscillator with the probe supplied was only from 8 to 22 Mc/s, it was now required to construct another probe head in order to cover the range below 8 Mc/s. Our probe was able to cover the range 3.5 Mc/s to 9 Mc/s.

The relationship between the proton resonance frequency and the value of the steady magnetic field is given by the

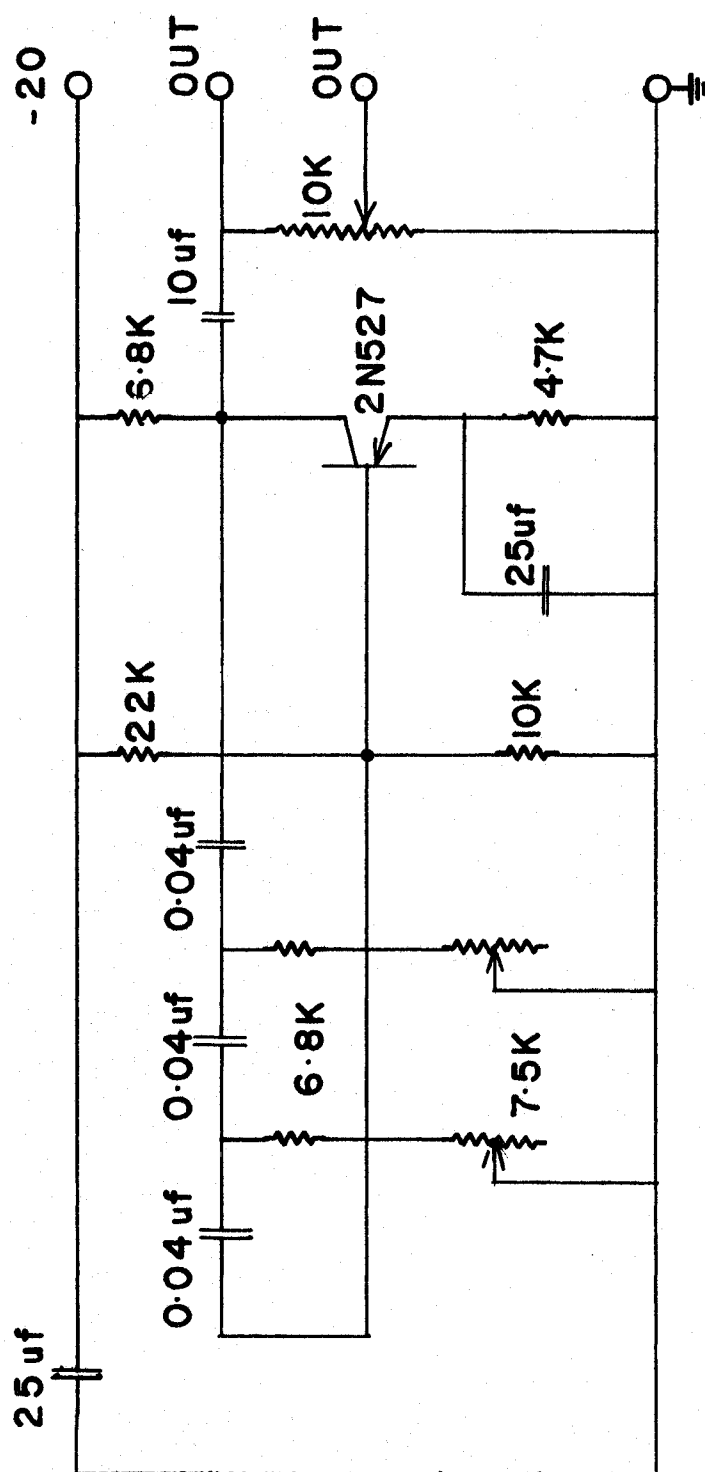


Fig. 11 200 c/s Oscillator

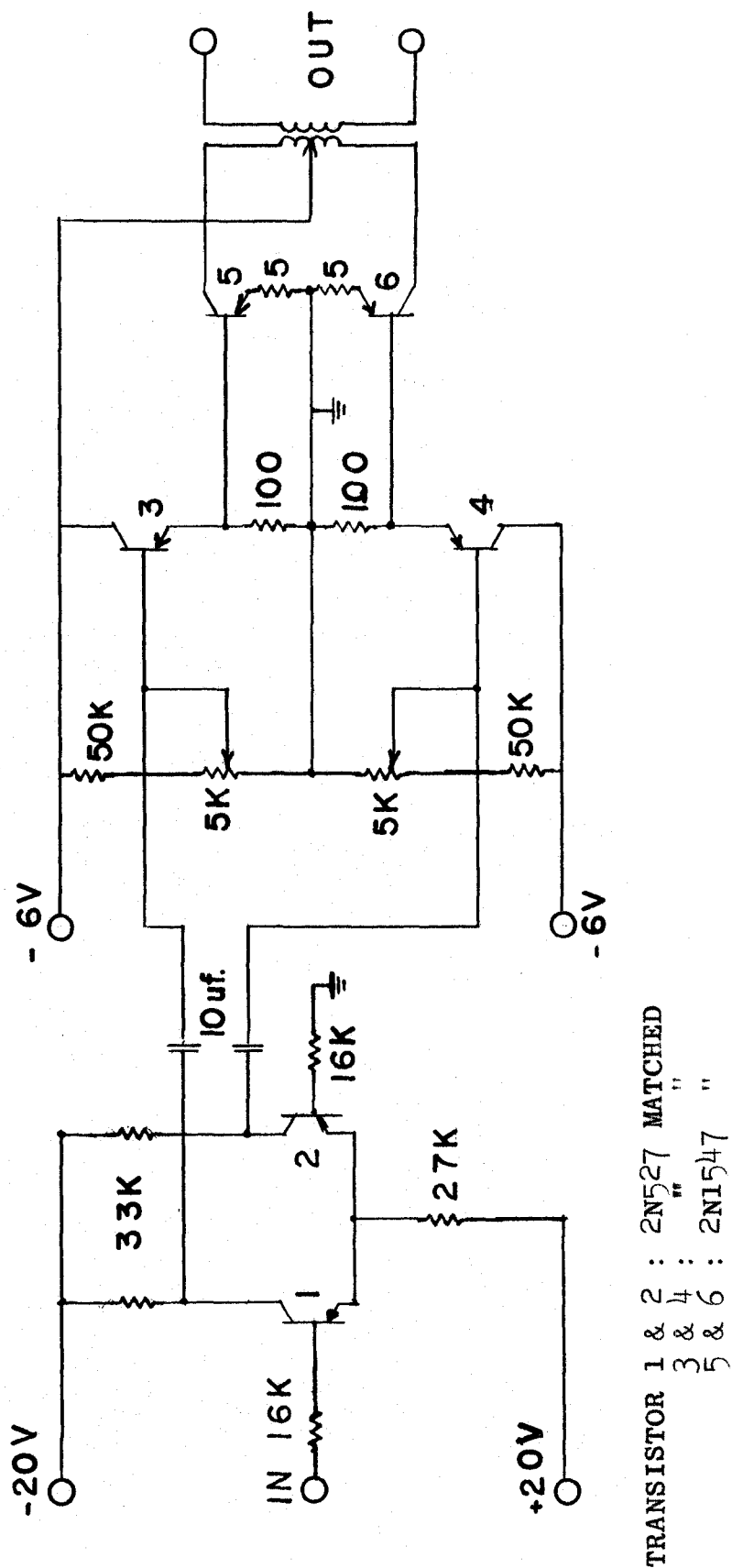


Fig. 12 Power Amplifier

equation:

$$h\nu = \gamma H \quad (1)$$

Since  $\gamma$  and  $h$  are well known and since  $\nu$  is the proton resonance frequency which was pre-set with the aid of a reference oscillator, then the magnetic field is from eqn. (1)

$$H = h\nu/\gamma \quad (2)$$

or 
$$H(\text{kgauss}) = \frac{1}{4.2577} \nu (\text{Mc/s}).$$

The reference oscillator used was a unit/time/frequency calibrator manufactured by the General Radio Company. The output frequencies of the reference oscillator covered the range from 10 kc/s upward in steps of 10 kc/s. The above frequencies were derived from a 5 megacycle quartz crystal oscillator whose frequency drift with temperature variation was  $-1 \times 10^{-7}/^{\circ}\text{C}$  to  $2 \times 10^{-7}/^{\circ}\text{C}$  for the ambivalent range  $20^{\circ} - 40^{\circ}\text{C}$ .

The experiment was performed at temperatures close to that of liquid air. The liquid air cryostat is shown in Figs. 13 and 14. The cryostat sits on the table and protrudes through an opening in the table and is centered carefully between the pole faces of the magnet as shown in Fig. 1. The liquid air trap consisted of a cylindrical brass container with a brass tubing extension. The waveguide terminating in the cavity was passed through the liquid air trap and the temperature of the cavity was within a few degrees of that of liquid air. To break the thermal contact between the liquid air trap and the outer chamber of the cryostat, there was inserted between the trap and the cryostat lid a short length of a plastic waveguide coated with aluminium foil on the in-

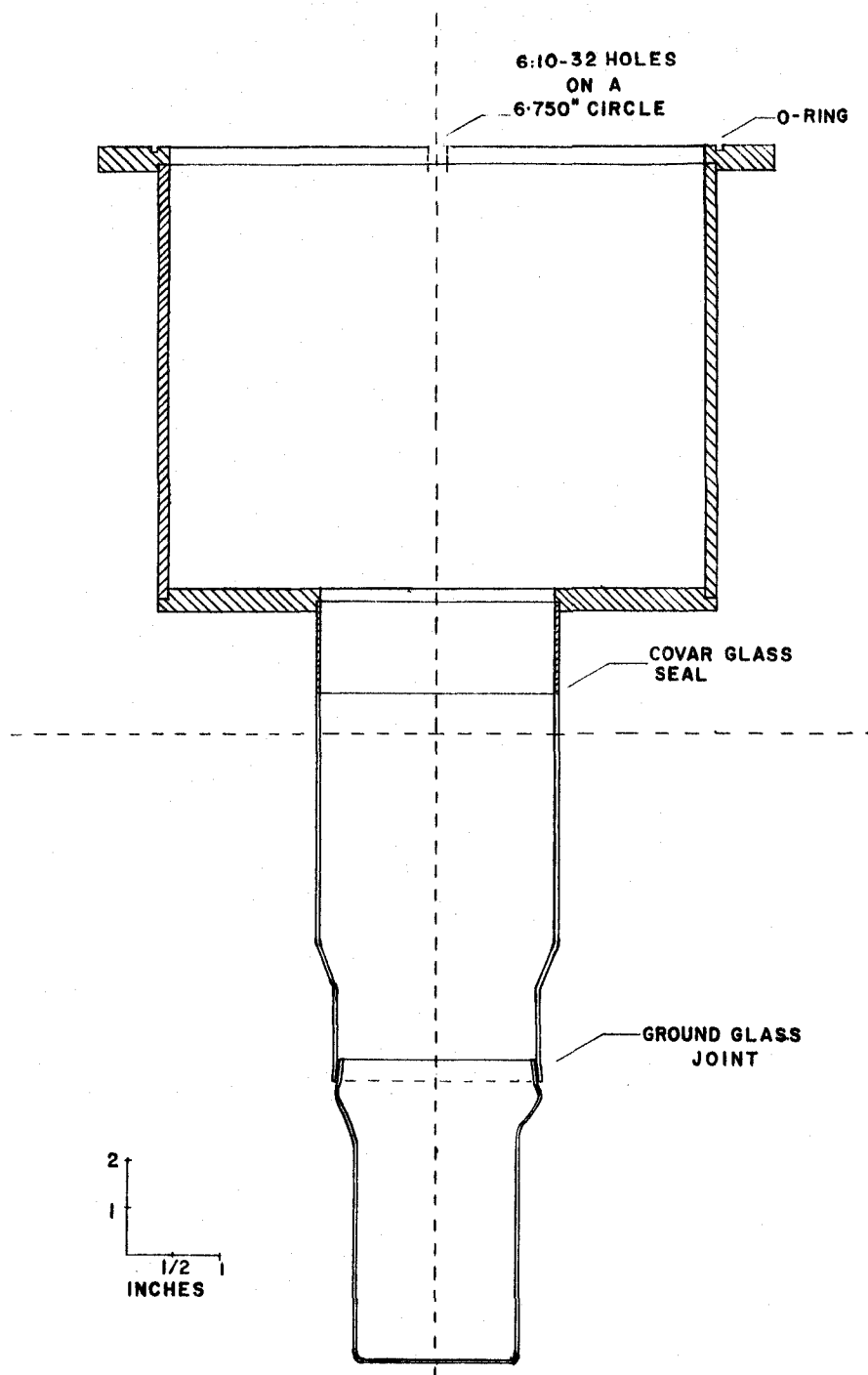


Fig. 13 Envelope of Cryostat

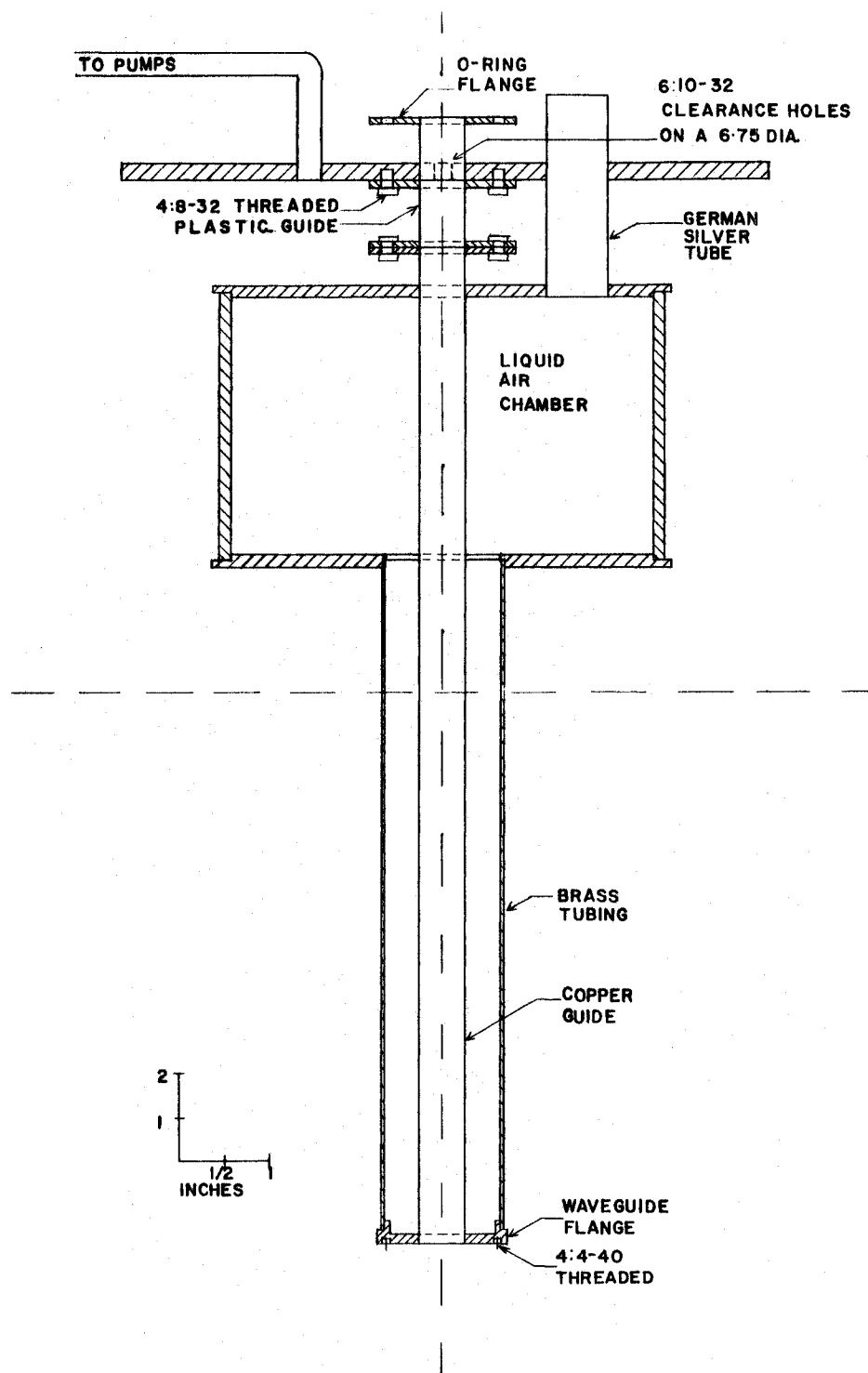


Fig. 14 Cryostat

side. Liquid air was introduced through a german silver tube as shown in the above figures.

To improve the thermal isolation, the cryostat was evacuated via a one half inch copper tubing which was equipped with a air admittance valve and a Pirani gauge head and was terminated by a small Consolidated Vacuum Corp. diffusion pump, model VMF-5. The diffusion pump was backed by a Welch Duo Seal mechanical pump.

All of the cavities that were used with this spectrometer were operated in the  $TE_{101}$  rectangular mode. The cavities were made from commercial X-band waveguide material. The cavities that were used to obtain the experimental results are shown in Fig. 15. With the crystal mounted the  $Q$  of the cavity was not less than  $3 \times 10^3$ . The cavities were coupled to the waveguide of the cryostat through a coupling plate made of  $10^{-2}$  inch thick copper plate and it had a coupling hole of approximately  $1/8$  of an inch in diameter.

The cavity used in the experiment on calcite had a section of its E-plane wall removed and its place was taken by a carefully machined copper plate H, which fitted snugly into this removed section. A calcite crystal that was under investigation was glued to this plate. In this way the crystal could be removed and mounted on the x-ray machine for irradiation without disturbing the crystal orientation or the coupling between the waveguide and the cavity.

The cavity used in the experiment on spodumene was equipped with a precision made goniometer which served to



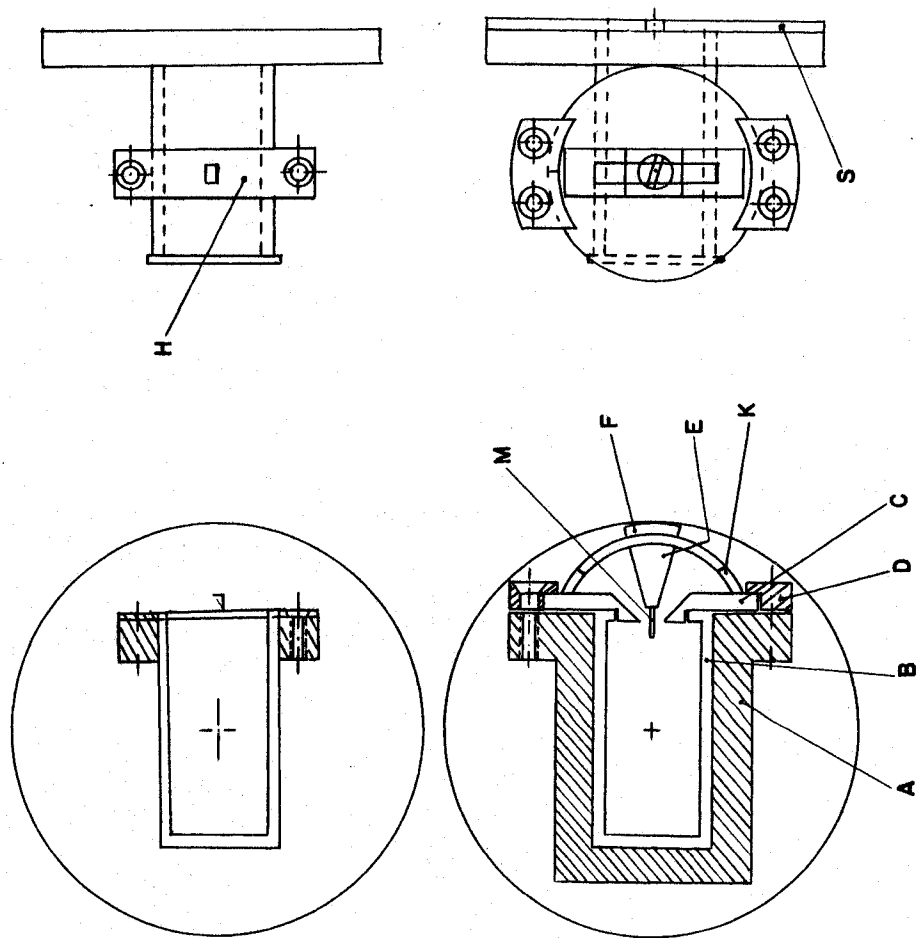


Fig.15 CAVITIES

orient the crystal accurately with respect to the cavity walls. The goniometer C, was fastened to the E-plane wall by means of a brass bracket composed of the parts A and D. The graduated plate C, of the goniometer could be rotated through 360 degrees about an axis normal to the E-plane of the cavity B. A semi-circular track K was soldered to the graduated plate of the goniometer with its axis of rotation parallel to it. The track bore a brass runner which is composed of the parts E and F. A nylon pin M, to which the crystal is glued is mounted in this brass runner. This runner allows the crystal to be aligned so that there was no translation of the axis of rotation for the magnetic field when it was rotated.

To put the spectrometer into operation, one has to tune mechanically the signal and local klystrons to give maximum power outputs at the desired frequency. The signal klystron was modulated by a variable 60 c/s signal on its reflector plate and the reflected power from the cavity was viewed by means of a power take-off through a directional coupler. By adjusting the klystron cavity tuner and the reflector voltage the frequency of the cavity was centered in a maximum power mode. When the approximate frequency of the cavity was noted by means of the wavemeter, the modulation was removed from the signal klystron. In a similar manner the local klystron was tuned. The 30 Mc/s beat frequency from the detector next to the local klystron was easily detectable on the oscilloscope. This indication was centered in a mode of oscillation which gave a maximum power output.

Next, the balanced crystal mixer was balanced. As before the signal klystron was modulated and the output of each detector of the mixer was compared until the outputs balanced each other. This was accomplished by the adjustment of the matching stub in each side arm of the magic tee,  $T_2$ . Again the signal klystron was returned to normal operation but this time the signal frequency control loop was closed. The signal klystron was stabilized by varying the 4.5 volt continuous voltage dial on the battery bank until the frequency control locked on. Similarly the local klystron was stabilized. The cavity was matched by tuning the slide-screw tuner and the other devices in the bridge until a minimum was obtained in the d-c. output of the 1N34 diode of the 30 Mc/s amplifier and detector. The modulation of the signal klystron was kept as low as possible to ensure a better signal to noise ratio. Before any measurements were taken the equipment was allowed to stand approximately one to two hours and any fine adjustments were made that were needed. This allowed the temperature of the crystal to reach its minimum value.

The N.M.R. probe was placed as close as possible to the glass vessel containing the cavity and locked into position. The first frequency measurement was set on the marginal oscillator by beating with the one megacycle output of the reference oscillator. In this way as the magnetic field was swept each succeeding one megacycle marker was set on the marginal oscillator. The frequency markers were recorded

on the strip recorder by shorting the terminals of the recorder by means of a crude telegrapher's key. The point of coincidence between the marginal oscillator frequency and the value of the steady magnetic field is noted by viewing the resonance line on the oscilloscope which uses a 60 c/s external modulation.

Since the steady magnetic field is modulated at a small fraction of the line width, then for resonance the first derivative of the absorption signal is obtained and it is this that is recorded on the strip recorder.

The amplifiers and oscillators of the detection and modulation systems were all transistorized.

#### IV

#### EXPERIMENTAL PROCEDURE AND RESULTS

In the investigation of calcite, one was interested in the effect of intense x-rays on the structure of the crystal lattice and whether the effect could be detected by paramagnetic resonance techniques. The changes in the dielectric and optical properties of calcite produced by the x-ray irradiation at normal temperatures has been studied by K. V. Rao (1961). He has reported that upon irradiation by x-rays calcite exhibited optical absorption in the ultra-violet region beyond 400 m $\mu$ . Also the dielectric loss of calcite increased considerably upon irradiation and there was a very strong thermoluminescence peak at 85°C with minor ones at higher temperatures. When heated after irradiation the dielectric loss of calcite gave a maximum in the temperature range 70°- 120°C and beyond 230°C it behaved in a similar manner to that of non-irradiated calcite. Rao concluded that the changes in the dielectric loss and the first glow peak were possibly due to the thermal release of the trapped electrons. It was presumed that the trapped electrons were thermally raised to the conduction band and produced thermoluminescence in the process of recombination with the holes initially created by the x-rays. These holes in the conduction band that were supposedly produced by the x-rays were

studied by paramagnetic resonance techniques.

In the chemical analysis of the crystals of calcite both manganese  $\text{Mn}^{+2}$  and iron  $\text{Fe}^{+2}$  were found as paramagnetic impurities. It was expected that the spectrum of  $\text{Mn}^{+2}$  would be observed at near liquid air temperatures but not that of  $\text{Fe}^{+2}$  because of its excessively short relaxation time. It would be necessary to cool the crystal down to liquid helium temperatures before the spectrum of  $\text{Fe}^{+2}$  would be observed. The investigation of the paramagnetic spectrum of calcite due to the presence of the  $\text{Mn}^{+2}$  ion has been thoroughly investigated by Hurd, Sachs and Hershberger (1954). They reported that the spectrum of this particular manganese ion consisted of thirty well resolved resonance lines, approximately 3.5 gauss in width and extended over a steady magnetic field range of 1100 gauss beginning at approximately 2500 gauss. A microwave frequency of 9300 Mc/s was used. Since the  $\text{Mn}^{+2}$  ion had a ground state  $^6\text{S}_{5/2}$  and a nuclear spin  $I = 5/2$ , then the total number of levels were  $(2S + 1)(2I + 1) = 36$ . Since the selection rules gave  $\Delta M = 1$  and  $\Delta m = 0$ , then there were allowed thirty transitions. The g-factor was found to be essentially isotropic; the hyperfine structure factors  $A'$  and  $B'$  were found nearly equal and the fine structure constants  $D'$  and  $d'$  were determined. The values found were:

$$\begin{array}{lll} g_{\parallel} = 2.002 & g_{\perp} = 2.0014 & A' = 8.782 \times 10^{-3} \text{ cm}^{-1} \\ D' = 3.75 \times 10^{-3} \text{ cm}^{-1} & & d' = 4.00 \times 10^{-6} \text{ cm}^{-1} \\ B' = 8.774 \times 10^{-3} \text{ cm}^{-1} & & \end{array}$$

The crystals of calcite investigated came from three different parent samples. They differed in their colouring and in their transparency. All of the calcite samples were prepared by cleaving them along the natural rhombohedral cleavage planes. The dimensions of all the sample crystals were approximately 5x5x2 millimeters. They were all, except for one, mounted in the same orientation. This one crystal was mounted with its crystallographic axis parallel to the axis of rotation of the magnetic field. This particular mounting was determined by a crystal goniometer. Each calcite crystal was irradiated at room temperature and in the dark. The crystals were irradiated for not less than 10 hours with the most energetic and most intense x-rays available (at 50 kilovolts and 20 milliamperes). The mounting for x-ray irradiation of the calcite crystals was flush against the exit slit of the x-ray tube. All irradiated crystals were mounted on the cavity plate while in the dark and under a red safe light. Then they were immediately inserted in the spectrometer and their spectra taken. Spectra were taken at both room temperature and a near liquid air temperatures. All resonance spectra for calcite were taken as the steady magnetic field was swept at a rate of 0.5 gauss/sec. and at a modulation frequency of 200 c/s with a peak to peak amplitude of 8 gauss.

One watched for a change in the resonance spectra of  $\text{Mn}^{+2}$  in calcite. Unfortunately the observed spectra showed no effects that could be attributed to the x-ray irradiation.

A strong luminescence as reported by Rao in 1961 was observed and also the resonance spectrum for the manganese ion as reported by Hurd, Sachs and Hershberger in 1954 was observed. All the sample crystals of calcite gave similar spectra.

It could be concluded that if there were paramagnetic entities present that it was possible that the temperature (liquid air temperature) at which the experiment was performed did not permit the Zeeman levels to be adequately populated to give an observable effect. An experiment at liquid helium temperatures would certainly correct this condition. Also it was thought that the relaxation time of the spin system may be insufficiently long and thus the resonance line would be broadened and obscured. Also an experiment at liquid helium temperatures would make possible the observation of resonance. Finally, it was thought that there may not be any paramagnetic entities produced by the irradiation of calcite.

In the investigation of spodumene the interest was in the paramagnetic features of the impurities in the single crystal. Spodumene has previously been thoroughly investigated by the nuclear electric quadrupole resonance method. Volkoff, Petch and Smellie (1952) have performed experiments on the splitting of the  $\text{Li}^7$  nuclear absorption lines in a single crystal of  $\text{LiAl}(\text{SiO}_3)_2$ . They found that one of the principal axes of the field gradient tensor  $\nabla E$  at the site of the lithium nucleus has been found to coincide with the b crystallographic axis. The other two principal axes are



in the plane of  $a$  and  $c$ .

The spodumene crystal ( $\text{LiAl}(\text{SiO}_3)_2$ ) is a monoclinic pyroxene with diopside structure. Its space group is  $C_{2h}^6$ . By the data of Warren and Biscoe (1931) and also Wykoff (1957) the unit cell has four molecules. The projection of the crystal structure on the (010) plane is shown in Fig. 16. The dimensions of the unit cell are:

$$a = 9.50 \text{ \AA}, \quad b = 8.30 \text{ \AA}, \quad c = 5.24 \text{ \AA} \text{ and } \beta = 69^\circ 40'.$$

The atomic co-ordinates with respect to the crystallographic axes ( $\xi, \eta, \zeta$ ) expressed as fractions of the unit cell dimensions are:

$$\text{Li}(.00, -.31, .25), \text{Al}(.00, .09, .25), \text{Si}(.21, .41, .25),$$

$$\text{O}_1(.39, .41, .14), \text{O}_2(.13, .25, .35), \text{O}_3(.14, .49, .00).$$

There is a twofold rotation axis parallel to the  $b$  crystallographic axis and passing through the Li and Al positions at  $\xi = .0, \pm .5, \zeta = \pm .25$ . Symmetry centers are located at  $\xi = .0, \pm .5, \eta = .0, \pm .5, \zeta = .0, \pm .5$  and also at  $\xi = \pm .25, \eta = \pm .25, \zeta = .0, \pm .5$ .

The spodumene crystal investigated was taken from a sample which was optically transparent but had a yellowish coloration. The crystal which was analyzed by the N.R.C. laboratories was found to have a number of paramagnetic impurities belonging to the iron transition group. They were manganese, iron and titanium, however there was only a 0.05 % concentration of manganese and a lesser concentration of titanium. The most abundant paramagnetic ion (with a concentration of 0.2 %) was  $\text{Fe}^{+3}$ . It was expected to give a spectrum at 11-

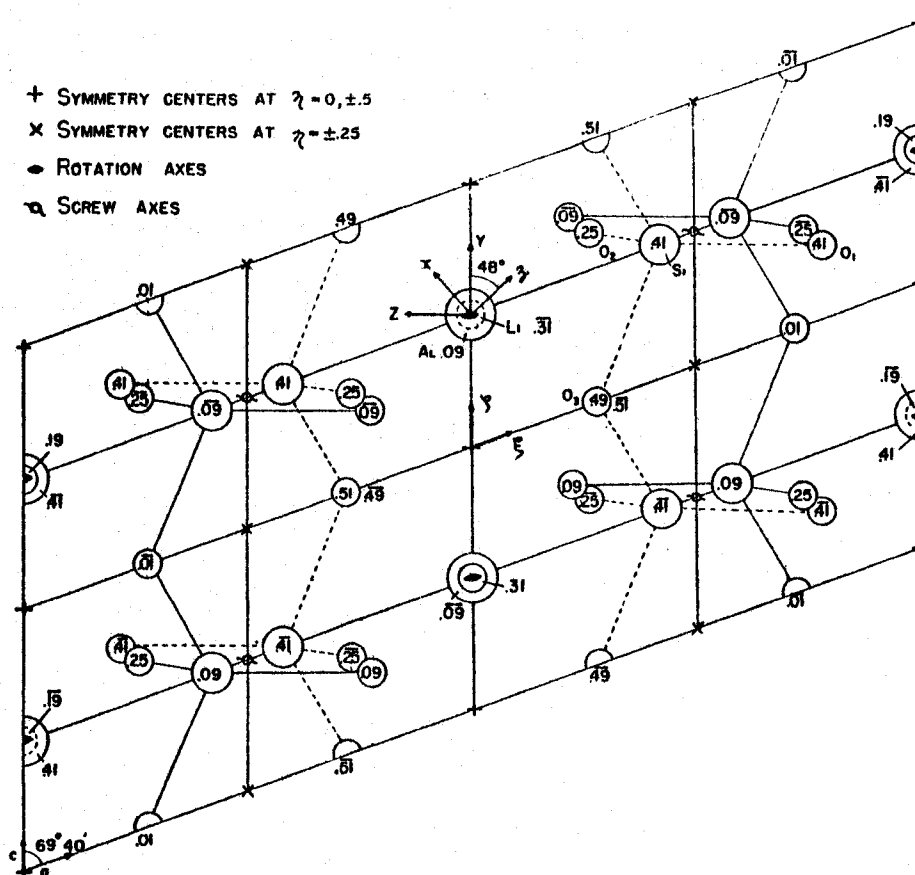


Fig. 16 Projection of a unit cell of monoclinic spodumene on the (010) plane.

quid air temperatures. A crystal of spodumene was taken from the sample in the form of a rectangular prism whose sides were formed by (110) cleavage planes. The intersection of the (110) planes defined the c crystallographic axis. The b crystallographic axis was taken to be in a plane normal to the intersection of the (110) planes. This obtuse angle as measured experimentally was  $96^\circ$ , whereas the calculated value was  $94^\circ$ . This angle was measured by optical means. The method involved the measurement of the angles between the beam of light reflected from the crystal faces.

In order to mount the crystal on the nylon pin of the goniometer, it was necessary to punch two very small holes in the crystal faces. The holes, approximately one millimeter in depth, were punched in the crystal by means of an ultrasonic drill; one was punched parallel to the  $b$  axis and the other was punched parallel to the  $c$  axis. To mount the crystal for the rotation of the magnetic field about the  $b$  axis, it was glued to the nylon pin in approximately the right orientation by the use of the hole parallel to the  $c$  axis. For the fine adjustment of the crystal so that its  $c$  axis was normal to the goniometer face the runner and the dial on the goniometer face was used. When the epoxy glue had dried the crystal was adjusted by moving the runner first. Following this operation the goniometer was assembled in the cavity. There now remained only the alignment of the  $b$  crystallographic axis with the axis of rotation of the magnetic field. To do this the cavity was placed under a microscope and a light was placed above the cavity. By means of reflections off the  $(110)$  planes, it could be ascertained when the angles between the  $(110)$  planes and the cavity walls were equal. When these angles became equal the goniometer face was locked by means of the set screws. For the rotation of the steady magnetic field about the  $bxc$  axis the graduated dial was rotated by ninety degrees in the  $E$ -plane from the position it held for the rotation of the field about the  $b$  axis and locked into position by means of the set screws. Finally, for the rotation of the magnetic field about the  $c$

crystallographic axis it was necessary to remount the crystal. In this case the crystal was glued to the nylon pin by the use of the hole punched parallel to the  $b$  axis. The plane of rotation of the runner at the time of glueing was made parallel to the H-wall of the cavity. After the glue had dried the cavity was placed under the microscope and any precession of the  $c$  axis in the H-plane was eliminated by adjusting the runner. In this way  $c$  was made parallel to the E-wall of the cavity. Finally any rotation of  $c$  found in the E-wall of the cavity was compensated for by the rotation of the graduated dial and in this way  $c$  was set parallel to the H-plane. These adjustments were made while the cavity was viewed with a microscope.

If  $bxc$ ,  $b$  and  $c$ , the axes about which the magnetic field was rotated, are denoted by  $x$ ,  $y$  and  $z$  then the data can be given in a right handed co-ordinate system. The spectrum with respect to each orientation was taken at  $15^\circ$  intervals and at a steady magnetic field sweep rate of 2.5 gauss/sec. The modulation frequency of the steady magnetic field was set at 200 c/s and the amplitude was set at 8 gauss peak to peak. All the spectra were taken at temperatures very near (within at least  $5^\circ$ ) that of liquid air. The data for the three separate rotations is tabulated in Table 1.

The angular variation of a single resonance line for the one half to minus one half transition is graphically presented in Fig. 17. The spectra for the three different orientations is presented on this one graph. For a rotation of the

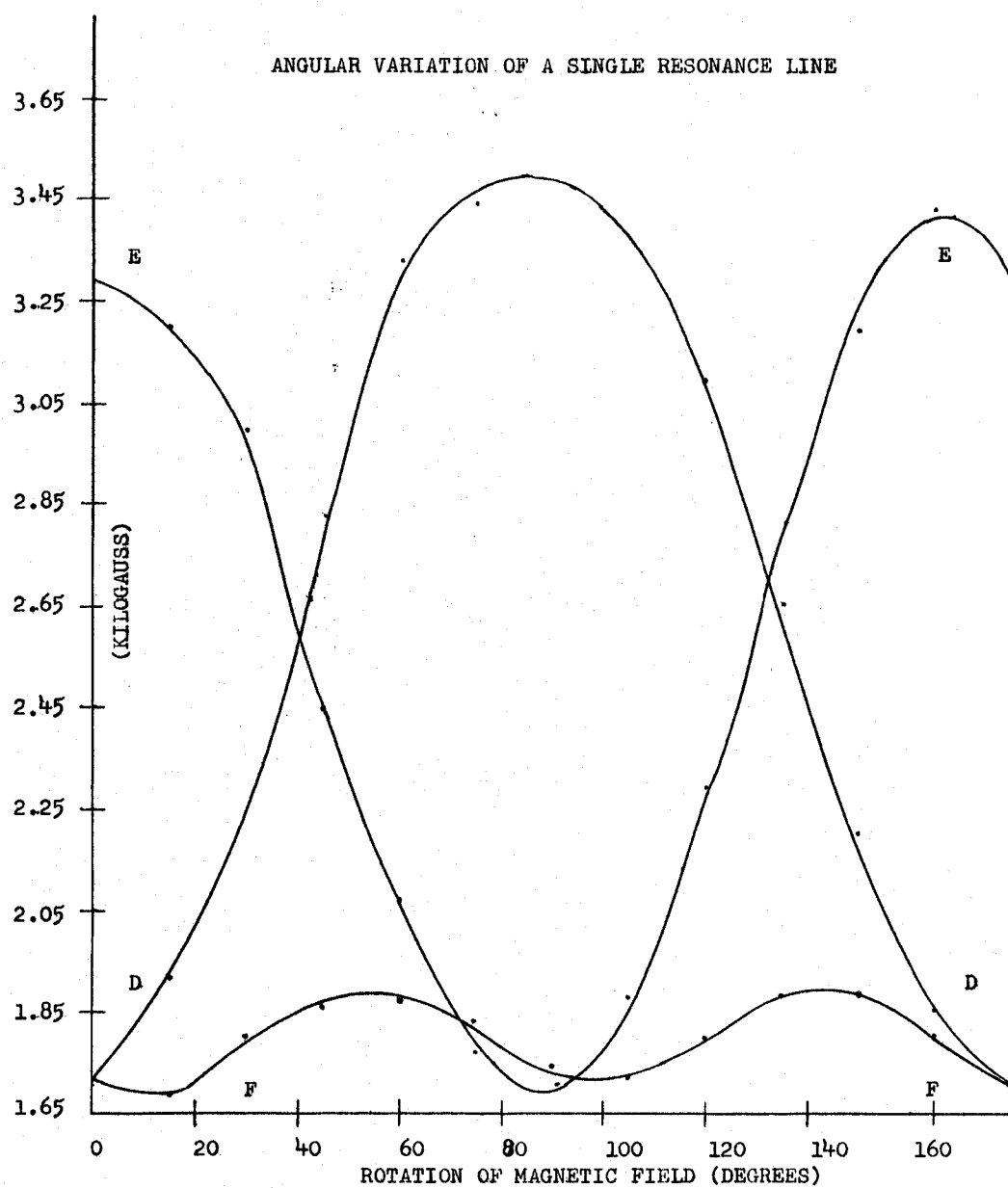


Fig. 17

TABLE I. DATA OF THE RESONANCE LINE FOR THE X Y AND Z ORIENTATIONS

$\theta$	X	Y	Z	Units
0	1.716 7.308	3.210 13.667	1.711 7.286	Kgauss Mc/s
15	1.931 8.225	3.085 13.136	1.689 7.193	
30	2.315 9.856	2.466 10.500	1.752 7.462	
45	2.831 12.053	2.080 8.859	1.861 7.923	
60	3.376 14.372	1.725 7.346	1.874 7.980	
75	3.433 14.820	1.680 7.154	1.834 7.807	
90	4.138 17.618	1.883 8.000	1.739 7.404	
105		2.317 9.866	1.729 7.364	
120	3.151 13.415	2.826 12.034	1.831 7.643	
135	2.657 11.315	3.194 13.600	1.888 8.040	
150	2.203 9.381	3.382 14.400	1.888 8.040	
165	1.849 7.876	3.295 14.031	1.803 7.679	
180	1.716 7.308	3.210 13.667	1.712 7.286	

steady magnetic field about the c crystallographic axis a straight line graph would be expected. This is because  $\theta$  is equal to ninety degrees and  $g$  becomes  $g_{\perp}$ . But by the graph there is present a small sinusoidal variation about the horizontal 1.8 kilogauss line. For the remaining two rotations of the steady magnetic field it is expected that the angular variation in the resonance line would follow the equation  $g^2 = g_{\parallel}^2 \cos^2 \theta + g_{\perp}^2 \sin^2 \theta$ . The graphs of these two crystal orientations do follow the same form as the above equation. From these two graphs it is possible to calculate the values of  $g_{\parallel}$  and  $g_{\perp}$ . This has been done and the results are listed in Table 2. Any angular variation in the  $g$ -factor caused by the crystal field has been ignored and only the relation  $h\nu = g\beta H$  for  $\Delta M = 1$  (1) has been considered. From equation (1) the value of  $g$  can be determined. Here  $h = 6.6252 \times 10^{-27}$  erg/sec,  $\nu = 8,952 \times 10^9$  c/s,  $\beta = 9.2732 \times 10^{-21}$  erg/gauss and the value of  $H$  is taken from the graphs. The values found for the two principal  $g$  directions are:

$$g_{\parallel} = 1.960 \quad \text{and} \quad g_{\perp} = 3.619.$$

There are also present in the spectra taken a number of other fairly strong lines that are part of the  $\text{Fe}^{+3}$  spectrum. Further the spectra exhibits a number of equally spaced and equally intense lines. This indicates a hyperfine interaction given by the interaction of the spin of the iron ion with that of the nuclear spins of both aluminium and lithium. Aluminium has a nuclear spin of  $5/2$  and lithium has a spin of  $3/2$ . The interaction of  $\text{Fe}^{+3}$  with these nearest neighbours can be

TABLE 2 DATA FOR THE CALCULATION OF  $g$  AND  $g$ 

Run	Axis of Rotation	Magnetic Field Value For $g$ (Kgauss) $g$	
D	X	1.716	3.500
E	Y	1.883	3.210
F	Z	1.800	
Average		1.799	3.355

expressed as:

$$\sum_N A_{Al} \vec{S}_{Fe} \cdot \vec{I}_{Al} + \sum_N A_{Li} \vec{S}_{Fe} \cdot \vec{I}_{Li},$$

where  $N$  is summed over the nearest neighbours of Al and Li.

The spectrum for  $Fe^{+3}$  is shown in Fig. 18.

Future plans include the theoretical calculation of the spectrum for  $Fe^{+3}$  with the crystalline field and the hyperfine structure included. Also the study of other diopside crystals will be undertaken.



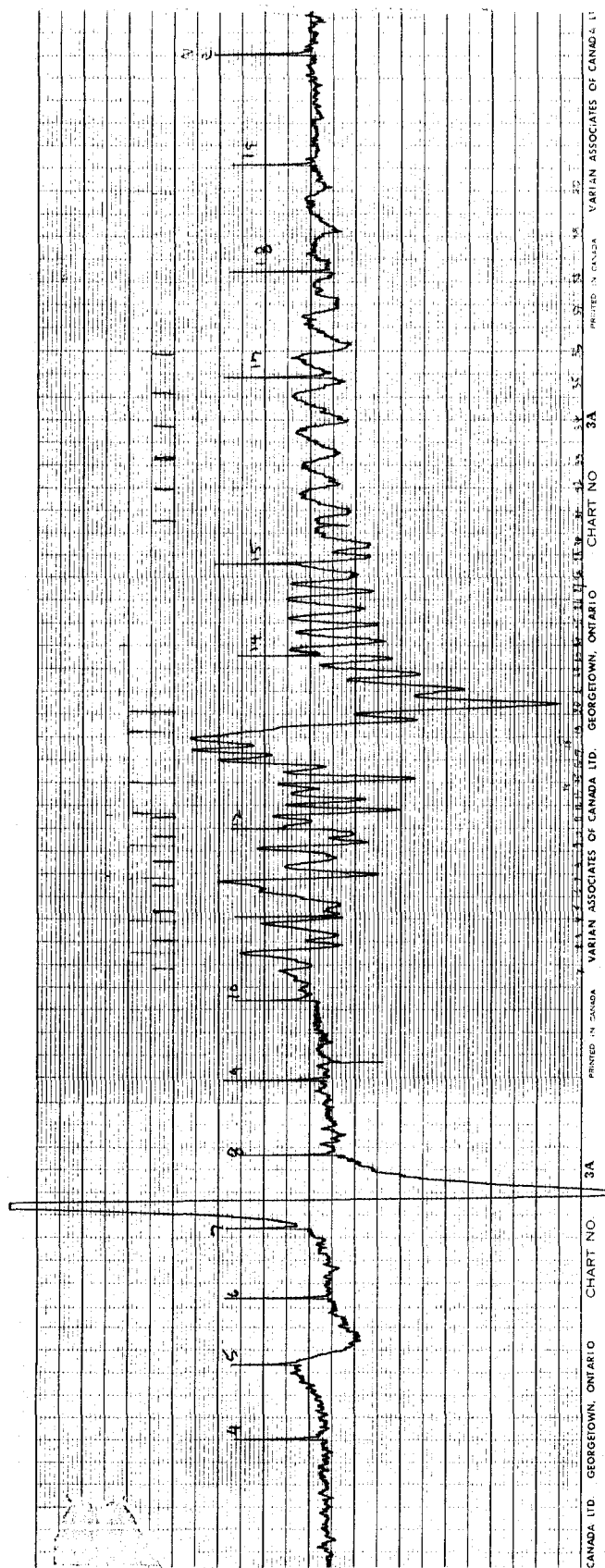


Fig. 18 The Resonance Spectrum of  $\text{Fe}^{+3}$  in Spodumene

## CONCLUSIONS

For this twofold study, we have reached a number of conclusions. We have summarized them below.

## (1) Calcite

The results for calcite were negative. There was no observed spectra that could be attributed to the effects of x-ray irradiation. This result suggests a number of possibilities.

- (a) there were no paramagnetic entities present;
- (b) if there were paramagnetic entities present, then it is possible that the Zeeman sublevels were not populous enough to give an observable effect at liquid air temperatures;
- (c) also, if there were paramagnetic entities present, then it is possible that the relaxation time of the spin systems was much too short and consequently the resonance line would be very broad and not easily detectable in the spectrum of  $Mn^{+2}$ .

The conclusions (b) and (c) could be very easily tested. Instead of doing the experiment at liquid air temperatures one could do it at liquid helium temperatures. The relaxation time would be lengthened and the population difference

between the Zeeman sublevels would be increased. The results of this experiment at liquid helium temperatures would either verify conclusion (a) or disprove it. Liquid helium was not available to us, therefore we were unable to carry out this experiment.

## (2) Spodumene

The paramagnetic resonance spectrometer recorded a spectrum for spodumene and we were able to draw a number of conclusions from it.

- (a) The paramagnetic spectrum can be associated with the  $\text{Fe}^{+3}$  ion.
- (b) The crystal field splitting is small because there is a number of resonance lines detected and not only the one that we analyzed.
- (c) The analysis on the single resonance line gave the values  $g_{\perp} = 3.619$  and  $g_{\parallel} = 1.960$  for the principal  $g$  values in a crystal of axial symmetry.
- (d) There is also present a hyperfine structure caused by the interaction of the nuclear spins of aluminium and lithium with the spin of the iron ion.

#### BIBLIOGRAPHY

- BAGGULEY, D. M. S. and GRIFFITHS, J. H. E. 1947 Nature 160, 532.
- BETHE, H. A. 1929 Ann. Physik 5 3, 133.
- CUMMEROW, R. L. and HALLIDAY, D. 1946 Phys. Rev. 70, 433.
- ELLIOTT, R. J. and STEVENS, K. W. H. 1953 Proc. Roy. Soc. A218, 553.
- FEHER, G. 1957 B. S. T. J. 36, 450.
- HURD, F. K., SACHS, M., and HERSHBERGER, W. D. 1954 Phys. Rev. 93, 373.
- JUDD, B. R. 1955 Proc. Roy. Soc. A227, 552.
- LOW, W. 1960 Solid State Physics Suppl., 2 Academic Press N.Y.
- RAO, K. V. 1961 J. Phys. Chem. Solids. 20, 193.
- VOLKOFF, G. M., PETCH H. E., and SEMLLIE, D. E. L. 1952 Can. J. Phys 30, 270.
- ZAVOISKY, E. 1945 J. Phys. U.S.S.R 9, 211.

#### VITA AUCTORIS

I was born in Windsor Ontario on February 25, 1937. I attended the Hon. J. C. Patterson Collegiate in Windsor and graduated from there in the spring of 1957. Then I took one year of engineering at Queens University, Kingston, Ontario. In the fall of 1958 I entered Assumption University and registered in the honours physics programme. I graduated from the university in the spring of 1962. In the fall of 1962 I registered in the graduate programme for physics. During my studies at the university I have held a bursary from the I. O. D. E., and one from the Independent Insurance Agents of Windsor.